ABSTRACT

Title of Document: EVALUATION AND IMPROVEMENT OF TEMPERATURE SENSITIVE PAINT DATA REDUCTION PROCESS THROUGH ANALYSIS OF TUNNEL DATA

Pratik Bhandari, Master of Science, 2012

Directed By: Professor Kenneth H. Yu, Department of Aerospace Engineering

A data reduction process for a temperature sensitive paint heat transfer measurement system in use at the US Air Force Hypervelocity Wind Tunnel No. 9 has been evaluated using a set of data gathered from tests on a generic hypersonic waverider model. Discrepancies were observed between heat transfer results calculated using temperature sensitive paint based measurements as compared to results calculated using conventional thermocouple measurements at specific locations on the test article. Paint thermophysical property estimates were made and utilized in a series of finite element models to analyze paint behavior. These models were used to perform a sensitivity analysis on system parameters. Key identified parameters were used to perform a non-dimensional analysis of the tunnel data. Based on this analysis, discrepancy areas were identified and a novel two-calibration data reduction process was developed that mitigated the severity of some observed discrepancies and showed the potential for future improvements.

EVALUATION AND IMPROVEMENT OF TEMPERATURE SENSITIVE PAINT DATA REDUCTION PROCESS THROUGH ANALYSIS OF TUNNEL DATA

By

Pratik Bhandari

Thesis submitted to the Faculty of the Graduate School of the
University of Maryland, College Park, in partial fulfillment
of the requirements for the degree of
Master of Science
2012

Advisory Committee:
Professor Kenneth H. Yu, Chair
Professor Christopher Cadou
Professor Raymond J. Sedwick

Acknowledgements

I would like to thank Ms. Inna Kurits, Mr. Joseph Norris, Mr. John Lafferty and the entire AEDC Hypervelocity Wind Tunnel No. 9 team for allowing me to conduct this research. I would also like to thank AEDC Hypervelocity Wind Tunnel No. 9, Mr. Lafferty and Mr. Dan Marren for sponsoring my research. I also greatly appreciate the help provided by my advisor Dr. Kenneth H. Yu. Without their support and guidance, this work would not have been possible. Special thanks to my friends and family for helping me throughout my entire academic career.

Table of Contents

List of Tables

List of Figures

List of Symbols and Abbreviations

Symbols

α	Thermal diffusivity
Δx	Nodal thickness
ρ_∞	Freestream density
μ	Dynamic viscosity
h	Convective heat transfer coefficient
k	Thermal conductivity
$\dot{q}_x$	Heat flux in the x direction
Bi	Biot number
C_p	Specific heat
E_{nr}	Activation energy for non-radiative process
Fo	Fourier number
H_o	Total enthalpy
I	Emission intensity
L	TSP thickness
L_c	Characteristic length
R	Universal gas constant
Re	Reynolds number
St	Stanton number
T	Temperature
U_∞	Freestream velocity

Abbreviations

AEDC	Arnold Engineering Development Complex
CCD	Charge coupled device
CFD	Computational fluid dynamics
TSP	Temperature sensitive paint

Chapter 1: Introduction

1.1: Motivation

Aerodynamic heating is a particularly important design factor for vehicles operating at hypersonic conditions. Modern design processes rely increasingly on computational fluid dynamics (CFD) tools; however, the models produced by CFD codes must be validated through comparison with experiment data. To that end, testing at the Arnold Engineering Development Complex (AEDC) Hypervelocity Wind Tunnel No. 9 (Tunnel 9) produces aerodynamic force, moment and pressure data as well as heat transfer data for specifically instrumented locations on the model. Traditional methods of determining heat transfer data involve the use of discrete sensors such as thermocouples or thin-film heat transfer gauges at specifically instrumented locations. These methods are mature techniques that have successfully been used in previous work; however, there are limitations inherent in the use of these methods.[1,2,3] Important flow phenomena including boundary layer transition, flow separation, and shock-shock interaction, among others, are difficult to detect unless some prior knowledge of the flow behavior is available. Specifically for hypersonic testing, flow behavior is not as well-known as for other flow regimes. This results in either an incomplete visualization of the flow or costly and labor-intensive instrumentation of the model. Additionally, certain areas of the model such as leading edges may be difficult to instrument appropriately.

To address these issues, Tunnel 9 has recently developed the capability to measure heat transfer using a novel intensity based temperature sensitive paint (TSP)

system.[4] TSP is one of a number of non-intrusive global measurement techniques that can be used to provide qualitative and quantitative data over the entire imaged area of the model. Similar paint-based measurement techniques have been used at Tunnel 9 and other facilities to measure temperature and pressure data.[3,5,6,7,8] A version of this system has been used to successfully produce quantitative heat transfer maps for previous tests at Tunnel 9 including pitching runs on a wedge model in Mach 10 flow.[6] Tunnel runs have also been carried out using a two-color TSP system. This two-color TSP system and the data reduction process are the focus of the present work.

A set of tunnel data collected on a model of a generic hypersonic vehicle has been analyzed in an effort to evaluate and improve the TSP data reduction process currently used at the facility. The data were used to determine the effects of paint thermophysical properties, paint layer thickness and applied heating load on the resultant heat transfer data determined from the TSP data reduction process. Specific to this work, efforts were made to determine the cause of occasional discrepancies between heat transfer results determined from the TSP data reduction and heat transfer results determined from performing data reduction on a set of thermocouple measurements concurrently made on the model. Possible mitigating actions to reduce these discrepancies were determined as well.

1.2: Global Temperature and Heat Transfer Measurement Techniques

Global measurement techniques specifically designed for temperature and heat transfer measurements have been in use since the late 1960's. Some typical

examples of these techniques include liquid crystals, infrared camera imaging, thermographic phosphors and temperature sensitive paints. Each method has its own set of advantages and disadvantages which will be briefly described here. Further information on these methods is given in Ref. 4.

Liquid crystals have been used to measure temperature and shear stress in a variety of flow conditions, primarily in low-speed flows with low heat flux. However, there have been successful uses of liquid crystals for qualitative and quantitative temperature measurements in hypersonic flows as well.[9] Liquid crystals are substances with unique molecular structures that are neither crystalline solids nor isotropic liquids. Chiral nematic liquid crystals in particular react to changes in temperature by changing color, allowing for liquid crystal thermography.[9] When performing liquid crystal thermography, the model surface is coated with a thin layer of the liquid crystals and illuminated with a white light source. The reflected color is a function of the temperature of the crystals allowing the calculation of heat transfer using appropriate data reduction techniques. The technique has the advantages of being straightforward and cost-effective; however, the crystals have major disadvantages specifically when dealing with hypersonic flows. For instance, the band of temperature for which the liquid crystals change the reflection color is narrow – no more than O(10°C) – and not suited for models where a large temperature span is required. Furthermore, the crystals typically exhibit a longer response time than other global measurement techniques – minimum response times are O(3 ms) – and this property can limit the temporal resolution of liquid crystal thermography.[10]

Infrared imaging is another widely used global temperature measurement technique. Chief among its advantages is the fact that little to no modification of the model is required to utilize this measurement. Global temperature measurements on the shuttle orbiter at hypersonic speeds during flight have been obtained using infrared images.[11] Infrared imaging determines the temperature of an object based on the emitted electromagnetic radiation of a given object as the emission power is proportional to T_{obj}^4. Knowledge of the surface temperature and appropriate data reduction techniques allow for the calculation of heat transfer. Infrared imaging can be used over large temperature ranges and modern imaging systems have optical and temporal resolutions acceptable for use in wind tunnel facilities, however, there are some disadvantages associated with this method. Namely, the low signal-to-noise ratio for uncoated models limits the resolution of the temperature measurements. Specific to metallic surfaces, emittance values tend to be low and must be coated with flat black paint or other coatings to increase emittance.[12] Furthermore, extensive knowledge of radiative properties for the model and tunnel environment (i.e. model material emittance and tunnel window losses) is required for accurate measurements. Feasibility testing was carried out at Tunnel 9 to determine whether commercially available infrared imaging systems could be used to accurately measure surface temperature on prototypical customer models made from stainless steel. It was determined that accurate measurements of surface temperature would not be possible with commercial imaging systems because of the low emittance values produced by the uncoated stainless steel surfaces.[13]

Thermographic phosphor techniques utilize the sensitivity of emission intensity to temperature to function as a temperature measurement technique. Typically, thermographic phosphor formulations are suspended in a ceramic binder and sprayed onto a test article. The overall imaging system and processes are very similar to how TSP functions as a measurement technique as described in Section 1.3 below. A relative intensity based two-color thermographic phosphor technique was used to determine global qualitative heat transfer maps on high fidelity orbiter models at the NASA Langley Hypersonic Facilities Complex.[14] However, data reduction methods for phosphors have currently been limited to applications involving ceramic test articles and not for the stainless steel models typically used at Tunnel 9.

With technological advances in paint formulation and especially in scientific grade digital charge-coupled device (CCD) cameras, temperature sensitive paint techniques have become viable for high speed flow conditions like those at Tunnel 9.

1.3: Overview of TSP

TSP and its pressure measuring counterpart, pressure sensitive paint (PSP), operate on the same basic principles. Luminescent molecules termed "luminophores" are dispersed in a polymer host material or binder. This mixture forms a coating with a similar consistency to that of spray paints and can be applied to the model. TSP formulations are designed to provide measurement over a range of temperatures, with some specialized formulations capable of withstanding temperatures of 800°C.[15] TSP has been used on a variety of model materials, but specific to Tunnel 9, stainless steel models are used because steel is capable of surviving in the harsh testing environment

experienced by the test article and because the instrumented thermocouples used for calibration purposes require a stainless steel model material. Initially, the stainless steel model is coated with a thin white basecoat layer to enhance optical reflectance. Once the basecoat cures, the combined luminophore and polymer TSP mixture is painted over top in a thin coat and allowed to cure. As the polymer cures, the result is a smooth, hard coating on the surface where the paint has been applied. Multiple coats of the TSP are applied until the desired thickness is reached. For a given amount of incident illumination, thicker paint layers have the advantage of producing larger emittance values due to a larger number of luminophores contained in the layer and can produce higher signal to noise ratios in the photodetector.

Once the model is painted and placed in the test cell, the luminophores are exposed to the appropriate illumination (usually blue or ultraviolet light). Exposure to this illumination causes the luminophore electrons to transition to excited energy states. The excited luminophore electrons relax to their ground state in a radiative process called luminescence. The luminophores that undergo luminescence emit photons red-shifted relative to the illumination wavelength. For TSP, the excited energy states can also transition to the ground state in a radiationless process known as thermal quenching. Practically, this means that there exists an inverse relationship between the radiative emission and the temperature of the paint. By performing calibrations to determine the specific relationship for a particular formulation of TSP, quantitative measurements of temperature can be determined with knowledge of only the emission intensity. The application of quantitative temperature measurements based on TSP to measure aerodynamic heating in wind tunnel testing has been in use

since the 1960's.[16] The TSP system set-up specific to Tunnel 9 is explained in detail in Chapter 2.

There are four main components to any TSP system: an illumination source, a model prepared with the basecoat and TSP, a detector system and finally data acquisition and processing capability.[17] Numerous facilities have recently used similar TSP measurement systems to gather global temperature data. Studies were performed at Calspan-University of Buffalo Research Center (CUBRC) to determine heating caused by boundary layer transition at Mach 10 to Mach 18 on the Space Shuttle Orbiter.[18] CUBRC also carried out testing on an elliptic cone lifting body in a hypersonic flow field using thin-film TSP and PSP measurement techniques.[19] Subscale testing of the NASA Crew Exploration Vehicle was carried out at the NASA Langley Unitary Plan wind tunnel using TSP, among other measurement techniques.[20] TSP has been used to analyze the onset of turbulence caused by boundary layer transition on airfoil models and shock/boundary layer interactions in inlet flow.[21,22] TSP and its close counterpart, PSP, were also used to measure surface temperature, pressure and heat transfer coefficient on an obliquely impinging jet.[23] A version of TSP suitable for use in cryogenic facilities was also used at the European Transonic wind tunnel facility to detect transition at high Reynolds numbers.[24] The next sections describe the Tunnel 9 facility in detail and two-color TSP.

1.4: Tunnel 9 Facility Description

Tunnel 9 is a long duration blowdown hypersonic wind tunnel, a one of a kind facility that uses pure nitrogen as the working fluid and operates at Mach 7, 8, 10 and

14. Reynolds numbers ranging from 0.05 X 10^6/ft to 48 X 10^6/ft can be generated in the test section as seen in Figure 1 reproduced from Ref. 4. Tunnel 9 has a large test section measuring more than 12 feet long with a 5 foot diameter. Large scale models may be tested in the tunnel with concurrent force, moment, pressure and heat transfer data measurements with appropriate instrumentation. Furthermore, the test cell features a model support system which has the capability to dynamically pitch the model during a tunnel run from -5 to 45 degrees at a rate of 60 degrees per second. For operation at various Mach numbers, the tunnel has a set of interchangeable nozzles that are mated to the test cell. Mach 10 and 14 nozzles are 40 feet in length with a 5 foot diameter exit. The Mach 8 nozzle is also 40 feet in length but has a 35 inch diameter exit and operates as a free jet when mated with the 60 inch diameter test cell.

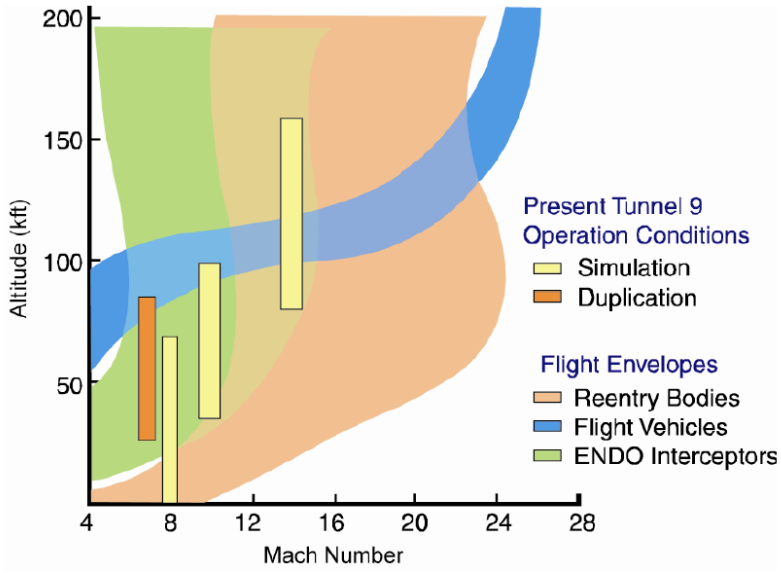

Figure 1. Hypervelocity Wind Tunnel 9 operational envelope.[4]

For any given run, the basic process the tunnel undergoes is the same. A bank of driver vessels containing the nitrogen gas working fluid is pressurized. The gas is then pumped into a vertical heater vessel. The heater utilizes a graphite heating element to heat the nitrogen to the appropriate pressure and temperature corresponding to desired freestream tunnel conditions. The test cell and vacuum sphere are evacuated to approximately 1 mmHg. Pre-scored metal diaphragms separating the heated, pressurized gas from the test section downstream are ruptured when the appropriate pressure and temperature for the working fluid is reached. The gas flows from the top of the heater vessel through the contoured nozzle and past the model located in the test section at the desired freestream tunnel condition. Cold nitrogen gas from the driver vessels is pumped simultaneously into the heater vessel. The cold gas operates like a piston, forcibly pushing all of the heated gas from the heater vessel. This allows the facility to maintain constant flow conditions in the test cell while a supply of the hot, pressurized gas is available. A schematic of the tunnel is shown below in Figure 2 reproduced from Ref. 4. The runtime is dictated by the fixed volume of high temperature and high pressure working fluid. A run is completed when the supply of hot, pressurized nitrogen is exhausted. The "good flow" portion of a run refers to the time interval where the desired run conditions are reached and maintained. Ref. 25 contains a more thorough account of the tunnel facility, its capabilities and processes.

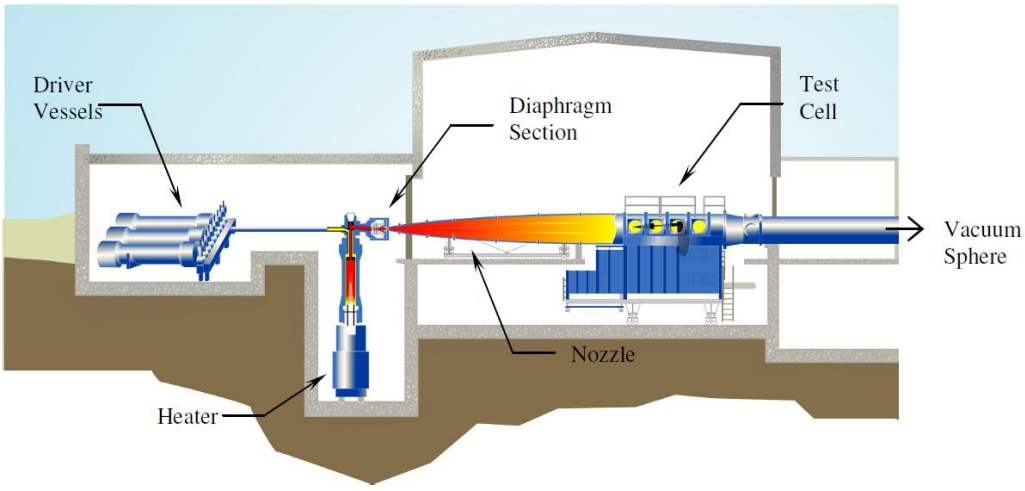

Figure 2. Tunnel 9 facility schematic.[4] Flow direction is left to right.

1.5: Two-Color TSP

A series of feasibility studies carried out in 2004 has led to the development of a robust TSP measurement technique at Tunnel 9.[26] The facility uses a two-color intensity based TSP measurement system to produce global quantitative heat transfer maps of a test article. Two-color TSP systems have the advantage of allowing for the correction of variations in the illumination field during the course of the run and, specific to Tunnel 9, allow for the capability to perform TSP measurements while dynamically pitching the model. Two-color TSP specifically means that the TSP formulation has not one, but two luminophores, each with the same excitation wavelength but with different radiative emission wavelengths. One of these luminophores is temperature insensitive and termed the "blue" luminophore for its emission wavelength centered at 450 nm. This luminophore responds chiefly to changes in incident illumination intensity. The other is temperature sensitive and

termed the “red” luminophore for its emission wavelength centered at 613 nm. This luminophore responds to changes in both incident illumination intensity as well as temperature. In this case, the luminophores used in the TSP formulation were excited by UV illumination at 365 nm. Prior work has been done using one color TSP using only the temperature sensitive – or red – luminophore in various facilities, and Ref. 4 focuses on the one color TSP system developed for use at Tunnel 9. A more complete description of the full data reduction process for reducing the two-color TSP data to heat transfer results is given in Section 2.3. Commonly used heat transfer data reduction methods can require accurate measurements of the thermophysical properties of the paint to produce results. This work uses methods developed in Ref. 4 to determine improved estimates of thermophysical properties used in finite element simulations to gain insight into the paint’s thermal behavior when coated on the model.

1.6: Research Objectives and Scope

The goal of the present work is to evaluate and improve the current data reduction process utilized at Tunnel 9 to convert global TSP temperature measurements to heat transfer results based on data gathered from a series of runs on a generic hypersonic waverider model. The work includes investigations into occasional discrepancies between the heat transfer results determined from TSP temperature measurements and results produced from traditional thermocouple instrumentation of the model, and possible techniques and methods to minimize the occurrence and magnitude of these differences.

Recently, a series of tunnel runs for a generic hypersonic waverider model were performed at Tunnel 9. The tunnel conditions spanned a range of flow Mach numbers, Reynolds numbers, various static angles of attack and also included dynamic pitching runs. The model was coated with TSP in an effort to measure global heat transfer on the model during the test. Data reduction was performed for the entire model to determine quantitative global heat transfer maps for the model based on the TSP measurements. The model was also instrumented with a small set of thermocouples to produce a standard set of heat transfer results. The current work was motivated by observed discrepancies in some cases between the heat transfer results produced by the TSP measurements as compared to the heat transfer results produced by thermocouple data. Figure 3 below shows an example of a plot comparing heat transfer results in the form of normalized Stanton number along a model cross-section determined from both TSP and thermocouple data. The TSP data and the thermocouple data were generally in good agreement for normalized location less than 0.6, but there were certain areas – specifically from normalized location 0.6 to 1 – where discrepancies existed between the TSP and thermocouple results. Thus, the main research objectives are

(i) to understand the physical mechanisms that lead to such discrepancies and

(ii) to develop an improved TSP data reduction approach on the basis of this understanding.

The improved data reduction approach can be used to identify any limitations in the traditional TSP data reduction algorithm and ultimately may lead to more accurate local heat transfer rate measurements in complex flow fields.

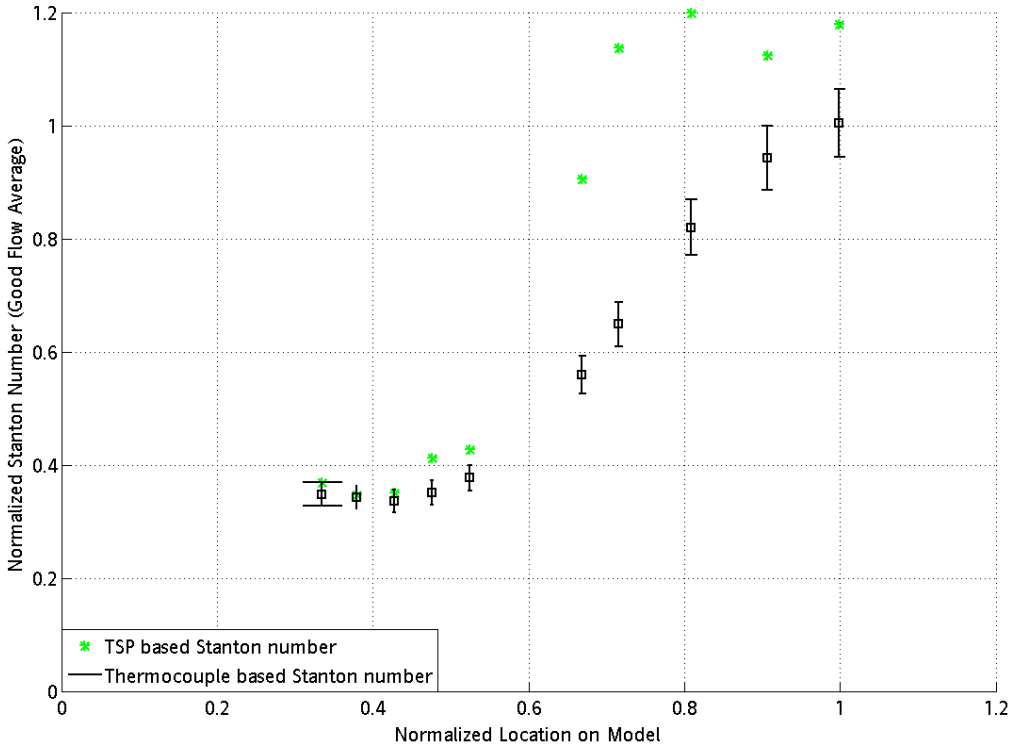

Figure 3. Sample of observed discrepancies between TSP and thermocouple heat transfer results.

Methods developed in a previous work were used on a larger, more complete data set to produce more accurate estimates of the thermophysical properties of the paint.[4] These thermophysical property estimates were used to perform simulations of the thermal behavior of the paint under idealized tunnel conditions using ANSYS, a commercial finite element modeling program. These simulations were used to perform a sensitivity analysis to determine the factors that most influenced the error

in heat transfer results based on the current data reduction method. A non-dimensional analysis of the most influential factors was performed on the data set to determine guidelines for when the current data reduction method would or would not produce discrepancies when comparing TSP based heat transfer results to thermocouple based ones. Finally, possible techniques and methods for minimizing these discrepancies were proposed and analyzed including a modified data reduction method incorporating the use of multiple *in-situ* calibrations. Future improvements to the data reduction process to further minimize discrepancies and expand capabilities are also discussed. The next chapter describes the TSP system in use at Tunnel 9 in more detail.

Chapter 2: Theory and Experimental Setup

2.1: Two-Color TSP

The TSP system used in Tunnel 9 utilizes a two-color TSP formulation and an intensity based measurement method. Specific to Tunnel 9, two-color TSP formulations are desirable because they allow global heat transfer results to be determined while the model is dynamically pitched during a run. Dynamic pitching of the model is a unique feature that Tunnel 9 can provide to the customer. Intensity based TSP methods rely on the illumination intensity and the corresponding emissive intensity of the TSP to determine temperature. An inverse relationship between emission intensity and temperature exists for any given formulation of TSP. This relationship can be written in the Arrhenius form and described by

$$ln\frac{I(T)}{I(T_{ref})} = \frac{E_{nr}}{R}\left(\frac{1}{T} - \frac{1}{T_{ref}}\right) \quad (1)$$

where $I(T)$ is the emission intensity at temperature T, $I(T_{ref})$ is the emission intensity at a reference temperature T_{ref}, E_{nr} is the activation energy for the non-radiative process and R is the universal gas constant.[27,28]

The TSP coating utilized for this series of tunnel runs was developed by LeaTech LLC. The coating consists of a mixture of the aforementioned luminophores in a binder or host material. The binder is a high-temperature polyurethane rated up to 360°F and the coating has been tested in lab calibrations up to 200°F. Typical TSP formulations have an uncertainty of ± 2°C over a temperature range of 20 - 100°C although experiments have shown uncertainty as low as ± 0.3°C using CCD cameras and where there is low relative motion between the test article and the illumination

source.[29,30] As the working fluid of the tunnel is nitrogen gas, there are no oxygen quenching pressure effects to account for and the Arrhenius form for the relationship between emission intensity and temperature given in Eqn. 1 can be used to produce a calibration to quantitatively determine temperature. A two luminophore paint does necessitate some changes into the basic equation; namely, rather than a single luminophore intensity ratio $I(T)/I(T_{ref})$, a ratio of ratios, $I_{ratioed}$, is used to allow for the blue luminophore to account for changes in emissive intensity caused by fluctuations in incident illumination rather than temperature. The ratio of ratios is calculated by

$$I_{ratioed} = \frac{\frac{I_{red}}{I_{red,ref}}}{\frac{I_{blue}}{I_{blue,ref}}} \tag{2}$$

where I_{red} and I_{blue} are the emissive intensities of the red and blue luminophores, respectively, and $I_{red,ref}$ and $I_{blue,ref}$ are the emissive intensities of the red and blue luminophores at a reference temperature. Qualitative temperature determinations can be made simply based on the relative levels of emissive intensity at various locations on the model, however, it is also possible to determine quantitative measurements of temperature at any given painted location. Quantitative temperature values can be determined by using a set of calibrations that relate emissive intensity to temperature. *A priori* lab calibrations and *in situ* calibrations determined from a small set of instrumented thermocouple locations can both be used for this purpose. In this context, each method delivers temperature measurements at slightly different locations. *A priori* lab calibrations provide TSP surface temperature whereas *in situ* calibrations provide measures of temperature at the interface between the paint coating and the model surface. *A priori* lab calibrations have been determined for a

series of TSP formulations at Tunnel 9.[31] However, evaluations comparing *a priori* calibrations and *in situ* calibrations for a pressure sensitive paint, similar to the TSP used at Tunnel 9, indicated that the *in situ* calibrations produced good agreement with tunnel pressure tap data.[32] Previous work at NASA Ames Research Center comparing TSP and thermocouple data for boundary layer transition has shown good agreement between the two sets using *in situ* calibrations.[33] Furthermore, previous TSP work at Tunnel 9 successfully used *in situ* calibrations.[4,6,8,34,41] The heat transfer results produced in this work were determined using *in situ* calibrations as well. *In situ* calibrations have successfully been used for a variety of heat transfer data reduction methods at other hypersonic facilities.[3,35]

Once the calibration is determined and applied, quantitative measurements of temperature are known for the entire imaged area. At this point, it is possible to determine heat transfer at the surface of the model using one of a number of heat transfer data reduction techniques. Temperature distributions and heat transfer rates for short duration flows can be solved for using constant heat transfer analysis equations; however, these methods are not appropriate for use in long duration flows such as those produced in tests at Tunnel 9.[35] Recent work has also investigated the use of analytical methods for determining heat flux from TSP data.[36,38] For the purposes of this work, a discretized version of the 1-D Fourier heat equation was used in conjunction with the TSP time history to determine heat transfer as follows:[38]

$$\dot{q}_x = \frac{k(T_1 - T_2)}{\Delta x} \tag{3}$$

where $\dot{q}_x$ is the heat flux in the x direction, k is the thermal conductivity of the material between station 1 and 2, T_1 and T_2 are the temperatures at station 1 and 2

respectively and Δx is the distance between station 1 and 2. This method has been used at Tunnel 9 previously and has also been used in many other hypersonic tunnels utilizing TSP due to its simplicity and relative accuracy.[35,37,38,39]

2.2: Hardware and Image Processing

Due to the unique test section environment experienced by models at Tunnel 9, models are usually made from stainless steel. Models made from stainless steel are able to withstand the large forces and moments generated during testing. Furthermore, stainless steel models make the use of stainless steel plugs for the thermocouple instrumentation unnecessary. Thermocouple measurements are sensitive to the surrounding substrate material. In this case, the thermocouples used for experiments conducted at Tunnel 9 have material properties that match the material properties of stainless steel. A model created from stainless steel allows for the thermocouple sensor and model combination to be treated as if it was a single material. Therefore, to reduce complexity and to negate the need for multiple models for a given test program, the TSP system in use at Tunnel 9 was developed with the stipulation that the system would use a stainless steel model. To accomplish this task, a coating of a reflective white basecoat layer and a coating of TSP must be applied to the model before the first test run. The white basecoat is used to ensure diffuse reflection of the paint emissions and not as an insulative layer as is typical in other TSP systems. Due to the uniquely long runtimes experienced by models tested at Tunnel 9, the required thickness for the insulative layer to prevent heat conduction to the metallic model is prohibitive.[4] The model preparation was finished by applying

successive coats of TSP until the desired thickness was reached. After the coating had been applied properly, the test article was marked with a series of black registration marks necessary for image registration purposes. For the data set analyzed in this work, the following components were used.

The illumination was provided by multiple Photon Technologies 200W mercury-xenon arc lamps. These lamps had been used successfully in previous tunnel runs that acquired TSP data. Originally, these lamps were chosen for their high stability characteristics. The lamp output was filtered with bandpass filters centered at 365 nm – the TSP excitation wavelength.

PI/Acton PhotonMax 512B cameras were used to capture radiative emission from the coated model. The cameras are low noise, scientific grade CCD cameras featuring a 512X512 pixel CCD array and a 16 bit A/D converter. These cameras were successfully used in previous work carried out at Tunnel 9. Specific to the present work, two cameras were used to capture the radiative emission, or one camera for each TSP color. As shown in Figure 4, a Custom Scientific dichroic beam splitter was used to allow both cameras to view the model simultaneously. The beam splitter allowed a greater than 95% transmission percentage for incident light with a wavelength greater than 590 nm and a less than 5% transmission percentage for incident light with a wavelength less than 560 nm. Therefore, the light emitted from the red luminophore at 613 nm passed through the dichroic beam splitter with minimal losses. The light emitted from the blue luminophore at 450 nm was reflected by the dichroic beam splitter. The cameras were further equipped with bandpass

filters tailored to ensure only emissions from either the temperature insensitive or temperature sensitive luminophores registered with the camera's CCD array.

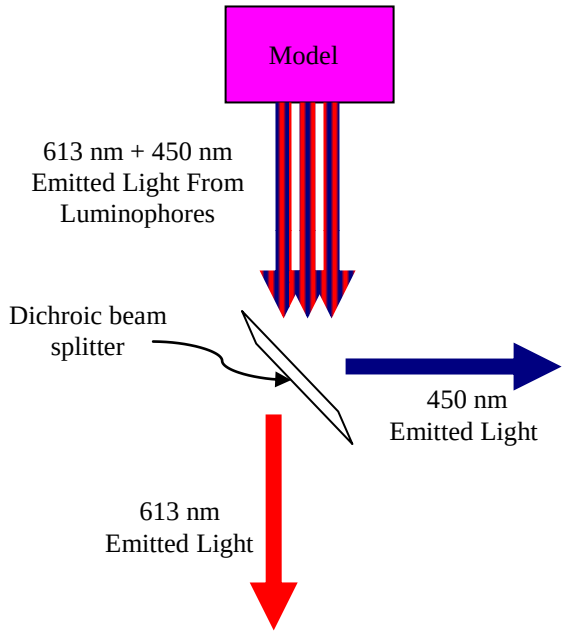

Figure 4. Simplified diagram of radiative emission path to camera CCD array from model.

After the test article was prepared with the appropriate coatings and registration marks, it was installed in the test section. The article was mounted on the test section sting mount. The sting mount was inserted into the aft section of the article. A balance measured force and moment data. The test article was illuminated with UV illumination provided by a set of four arc lamps filtered with bandpass filters centered at 365 nm. Scientific grade CCD cameras were used to acquire images of the article during the test as mentioned earlier. The test cell and equipment layout is shown below in Figure 5 reproduced from Ref. 6.

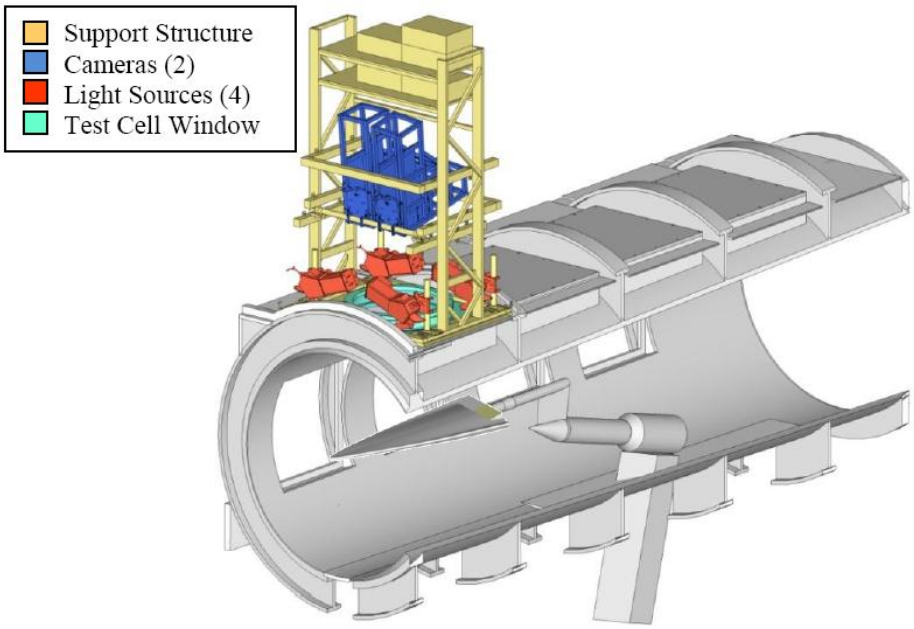

Figure 5. Tunnel 9 test cell and TSP equipment layout.[6]

Image data are acquired to successfully implement the TSP measurement technique. Corrections for dark current and ambient light were applied to the image by taking a so called “dark” image and subtracting from data images acquired during the run. The dark current is the term given to describe the electric current in a given photosensitive device when no photons are entering. Relative to typical emission values registered by the CCD cameras, the dark current is small, but non-negligible. Ambient light also affects the values registered by the camera. In practice, it is extremely difficult to completely eliminate all sources of ambient light during a run; therefore, a correction is applied to the data images to account for this effect. The dark image is acquired when the camera CCD chip is cooled to its operating temperature and all controllable light sources are turned off. After the data images had the dark image values subtracted from each pixel, the data images were mapped

onto a 3-D grid of the model using the image registration marks. This was necessary to build an accurate time history for a given location on the article over the course of the run. Once the images had been registered appropriately using the image registration marks as described above, basic image processing was performed. A reference image was chosen to determine the values necessary to determine the ratioed emission values ($I_{ratioed}$). The reference image is a wind-off image where the model is at a uniform initial temperature. Basic data processing involves ratioing the wind-on and wind-off images to correct for variations in paint thickness, luminophore concentration and illumination.

The paint coating thickness was measured in two ways. Initially, a Fischer Technology Dualscope MP40E-S fitted with an EGAW 1.3 right angle magnetic induction probe was used to measure TSP coating thickness. The magnetic induction probe uses magnetic induction to measure coating thickness of nonmagnetic coatings on ferrous metals – such as a TSP coating applied on the stainless steel models used in typical Tunnel 9 tests. This method has been used previously to determine coating thickness of pressure sensitive paints at the NASA Ames research center.[40] The probe was used to determine coating thickness for a number of locations on the model. However, model curvature and variations in the magnetic field caused by embedded instrumentation led to large variance in the measurements at a given location. The test article was partitioned into arbitrary sections based on key geometric features and an average coating thickness for each section was determined instead. This average section thickness provided an estimate with an uncertainty of ± 16%. After testing of the article was completed, the coating itself was peeled off in the sections of interest.

The thickness of the peeled TSP coating was then measured using a micrometer for a secondary thickness measurement.

2.3: TSP Heat Transfer Data Reduction

Tunnel 9's unique operational behavior results in the use of customized data reduction procedures. For example, unlike other hypersonic facilities, Tunnel 9 is not an impulse or shock facility, nor is the model injected into the flow. Therefore, a step change in heat transfer rate is not a valid assumption. Since the article is located in the tunnel during the entire start-up phase of the tunnel, a more appropriate model of the heating profile is ramp-like. Furthermore, since the tunnel has the ability to dynamically pitch the model during a run, the heating input on any given point on the model – usually a function of the angle of attack – can also vary with time. Traditionally, data reduction at Tunnel 9 using instrumented thermocouples has been accomplished by using a second order, Euler explicit, finite-difference approximation method to solve the transient 1-D heat equation.[4] The finite-difference approximation is subject to a convergence criteria expressed by Eqn. 4 below, where α is the thermal diffusivity of the wall material, Δt is the time step and Δx is the differential element size.

$$Fo = \frac{\alpha \Delta t}{\Delta x^2} < \frac{1}{2} \tag{4}$$

$$\alpha = \frac{k}{\rho C_p}$$

The thermocouple time history provides a temperature boundary condition at the model surface. The model is assumed to be at a uniform initial temperature and it is

also assumed that zero heat transfer occurs at the back wall. The back wall heat transfer assumption has been validated for models tested at Tunnel 9 thicker than or equal to 0.375 inches.[41] The finite difference method solves for the temperature at nodes throughout the steel model. Based on the heat conducted into the model, the local convective heat transfer rate can be calculated at the surface.

Ideally, the TSP coating could simply be modeled as an additional layer in the finite difference method; however, this requires accurate knowledge of the TSP thermophysical properties. The determination of these thermophysical properties is a non-trivial task and concurrent research seeks to establish these values. The current work also uses methods developed in Ref. 4 to produce improved estimates of these properties for use in a finite element model simulation of paint behavior as seen in Sections 3.2 and 3.3. Since the TSP thermophysical properties are not known precisely, the current data reduction process uses an *in situ* calibration assuming a linear temperature gradient through the paint layer to determine a relationship between the TSP emission intensity and the temperature at the interface between the paint and the steel model wall at that location. The method and underlying assumptions are treated in depth in Section 2.3.1 below. The paint and model wall interface temperature is used as an input into the same data reduction algorithm used to produce heat transfer results from thermocouple data. After the convective heat flux data is determined, it is usually non-dimensionalized into a Stanton number. The Stanton number measures the ratio of heat transferred into a fluid to the thermal capacity of the fluid and is used to characterize heat transfer in forced convection flows, such as wind tunnels. The Stanton number is defined as:

$$St = \frac{\dot{q}}{\rho_\infty U_\infty (H_o - C_p T_w)} \tag{5}$$

where ρ_∞ and U_∞ are the freestream density and velocity, H_o is the calculated total enthalpy, C_p is the specific heat of nitrogen at constant pressure and T_w is the measured wall temperature. Generally, thermocouple data produces heat transfer results with a quoted uncertainty of ± 6 percent for fully laminar or fully turbulent regions.[42]

The TSP coating is an insulator relative to the stainless steel model. Previous estimates of TSP thermophysical properties given in Ref. 4 indicate that the properties do indeed vary non-linearly with temperature. TSP thermal conductivity is orders of magnitude lower than the thermal conductivity of stainless steel. This can lead to heat storage issues inside the paint layer. The thickness of the coating is typically on the order of 2 mils and is generally accepted as being too thick to be thermally transparent, meaning that the effects of the coating cannot be ignored in the data reduction process.[43] Furthermore, due to the long duration and the ramp-like heating profile shown in Figure 6, the non-linear temperature-dependent thermophysical properties of the TSP coating must be accounted for in the data reduction. Estimating these properties is a non-trivial task so a successful data reduction process either utilizes accurately measured thermophysical properties over the range of temperature experienced during the run or bypasses this requirement in some way. A method developed in Ref. 4 uses an *in situ* calibration process to allow for data reduction without knowledge of the paint thermophysical properties.

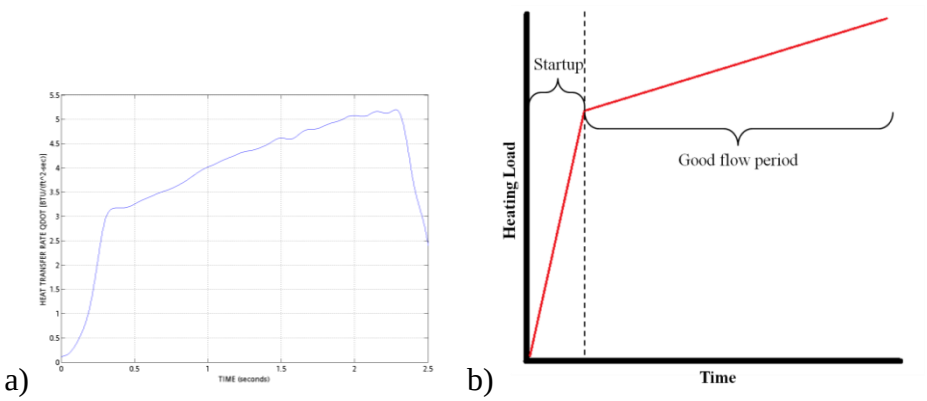

Figure 6. a) Actual heating profile for an instrumented location during tunnel run b) Idealized heating profile used for simulation purposes

2.3.1: *In Situ* Calibration Process and Assumptions

A simplifying assumption implying that the temperature gradient through the paint layer is linear is made. This assumption allows for the treatment of the comparatively thin TSP coating as a single layer rather than a series of differential elements as the thick steel model wall is treated in the data reduction algorithm. Schematically, the TSP coated test article is treated as seen in Figure 7 reproduced from Ref. 4.

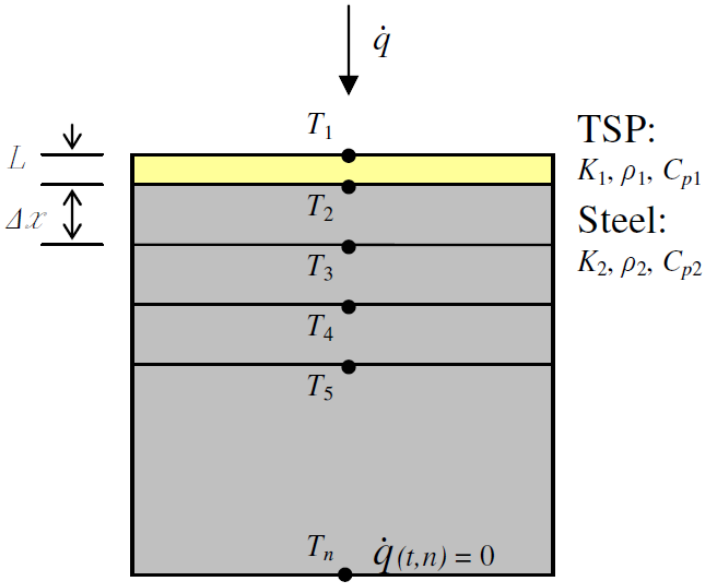

Figure 7. TSP and steel model wall schematic representation.[4]

This treatment of the model relies on the 1-D heat conduction assumption. This is a common assumption used when implementing TSP in hypersonic facilities. The assumption simplifies the data reduction process and maintains good relative accuracy.[35,37,39] This treatment works well for areas of the model where lateral conduction is negligible. Areas with large heating gradients or areas where model wall thickness varies as well as complex geometries like fins and leading edges require alternative methods. Robust treatments have been developed in recent works that are more adept at dealing with these cases, but they are outside the scope of this work.[37]

The *in situ* calibration requires a set of thermocouples to be instrumented on the test article. Ideally, these thermocouples are located such that they capture the entire range of temperatures experienced by the test article. After the thermocouples are instrumented, the entire test article – including the thermocouples – is coated with

the TSP. At the instrumented locations, a paint emission intensity and model surface temperature underneath the paint layer are known. Therefore, a calibration can be determined to relate paint emission intensity to model surface temperature beneath the coating. Applying this calibration globally produces a global temperature map indicating model surface temperature underneath the paint layer. The model surface temperatures over the entire imaged area are then treated essentially as if they were temperature time history data gathered from instrumented thermocouples. The model surface temperature is then used as a boundary condition for the standard data reduction algorithm used for coaxial thermocouple data at Tunnel 9. The advantage gained by the TSP coating is that rather than determining heat transfer results only at the instrumented thermocouple locations, a global heat transfer map can be determined instead. Note that this method requires no knowledge of the thermophysical properties of the paint, the coating thickness or even the temperature of the paint surface, and also that existing data reduction code can be leveraged to determine heat transfer results. A brief overview of the detailed justification of the data reduction method shown in Ref. 4 follows.

Referring to Figure 7 and applying Eqn. 3 above to the interface between the TSP coating and the model surface layer, we find:

$$\dot{q}_{TSP\ interface} = \frac{k_1(T_1 - T_2)}{L} \qquad (6)$$

$$\dot{q}_{Steel\ interface} = \frac{k_2(T_2 - T_3)}{\Delta x}$$

At this interface, $\dot{q}_{TSP\ interface} = \dot{q}_{Steel\ interface}$ so solving for k_1 results in:

$$k_1 = k_2 \frac{L}{\Delta x} \frac{(T_2 - T_3)}{(T_1 - T_2)} \qquad (7)$$

Note that the data reduction algorithm used by Tunnel 9 solves the one-dimensional transient heat equation (Eqn. 8) for nodal temperatures using the second-order, Euler explicit, finite difference approximation (Eqn. 9).

$$\frac{\partial T}{\partial t} = \alpha\left(\frac{\partial^2 T}{\partial x^2}\right) \tag{8}$$

$$\frac{\left(T_{i+1,j} - T_{i,j}\right)}{\Delta t} = \alpha\left(\frac{T_{i,j+1} - 2T_{i,j} + T_{i,j-1}}{\Delta x^2}\right) \tag{9}$$

$$\dot{q} = -k\left(\frac{\partial T}{\partial x}\right)_{surf} \tag{10}$$

$$\dot{q} = \frac{-k_1}{L}\left[-3T_{i+1,1} + 4\left\{\frac{1}{2}\left(T_{i+1,1} + T_{1+1,2}\right)\right\} - T_{i+1,2}\right] \tag{11}$$

Substituting the value for k_1 given in Eqn. 7 into Eqn. 11 and simplifying results in the following:

$$\dot{q} = \frac{k_2(T_2 - T_3)}{\Delta x} \tag{12}$$

This indicates that if the linear gradient assumption is valid, the *in situ* calibration method can be used to determine surface heat transfer values without prior knowledge of the coating thermophysical properties. Practically speaking, this method allows a calibration to be made using a small set of instrumented thermocouples to relate paint emission intensity to model surface temperature underneath the TSP coating. The paint emission intensity time history is converted to a model surface temperature time history using the *in situ* calibration. Some examples of *in situ* calibrations and common problems are presented below.

2.3.2: Calibration Examples and Problems

A set of thermocouples were instrumented on the test article. For each run, data recorded from the instrumented thermocouples were used in conjunction with the TSP emission data to produce calibrations relating paint emission intensity to model surface temperature below the TSP coating. A typical plot used to determine the *in situ* calibration is shown in Figure 8 below.

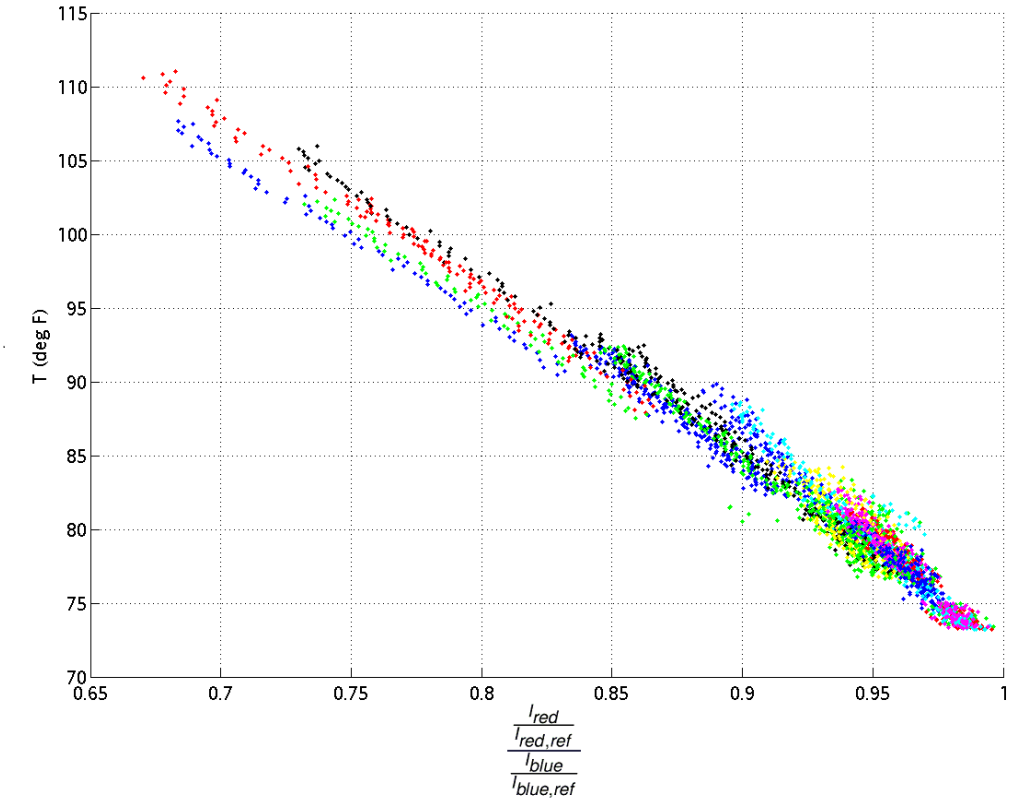

Figure 8. Typical model surface temperature vs. ratio of ratios plot used for *in situ* calibrations. Test Program 1: Run 4.

Each set of colored points corresponds to a different location on the model. Each of these locations has been instrumented with a thermocouple. On the y-axis, the model surface temperature underneath the paint layer is plotted. On the x-axis, the

ratio of ratios or $I_{ratioed}$ value for the pixel corresponding to that physical location is plotted. In general, the temperature and intensity plots follow the expected inverse relationship; namely, as the model surface temperature increases, the corresponding paint emission value decreases. To determine the calibration relationship, a subset of the instrumented locations is chosen such that it spans the range of temperatures experienced in the wind tunnel during the run. A straight line fit is applied to the data and is used to convert the paint emission intensities to model surface temperature. An example of such a plot is shown in Figure 9 below with the thick black line being the calibration curve.

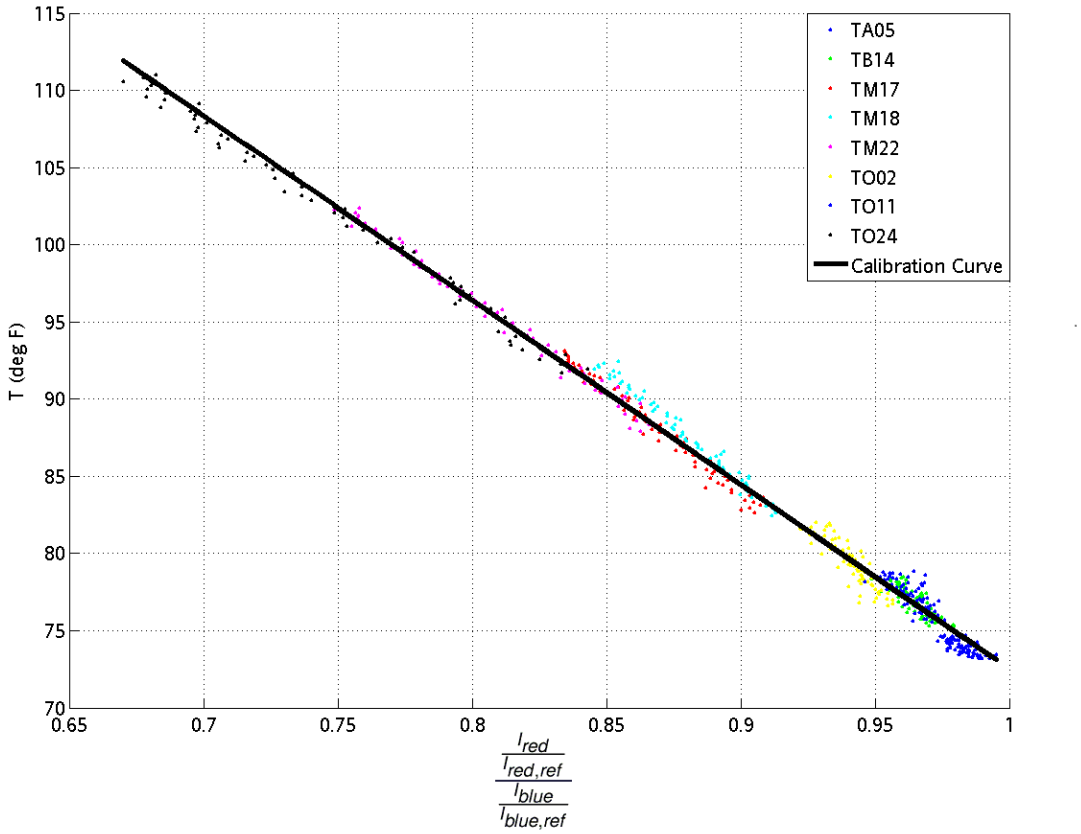

Figure 9. Subset of instrumented locations used to determine *in situ* calibration. Test Program 1: Run 4.

However, there are certain locations where the paint emission and temperature behavior is not appropriately approximated by the calibration curve. An example of this is shown in Figure 10 below.

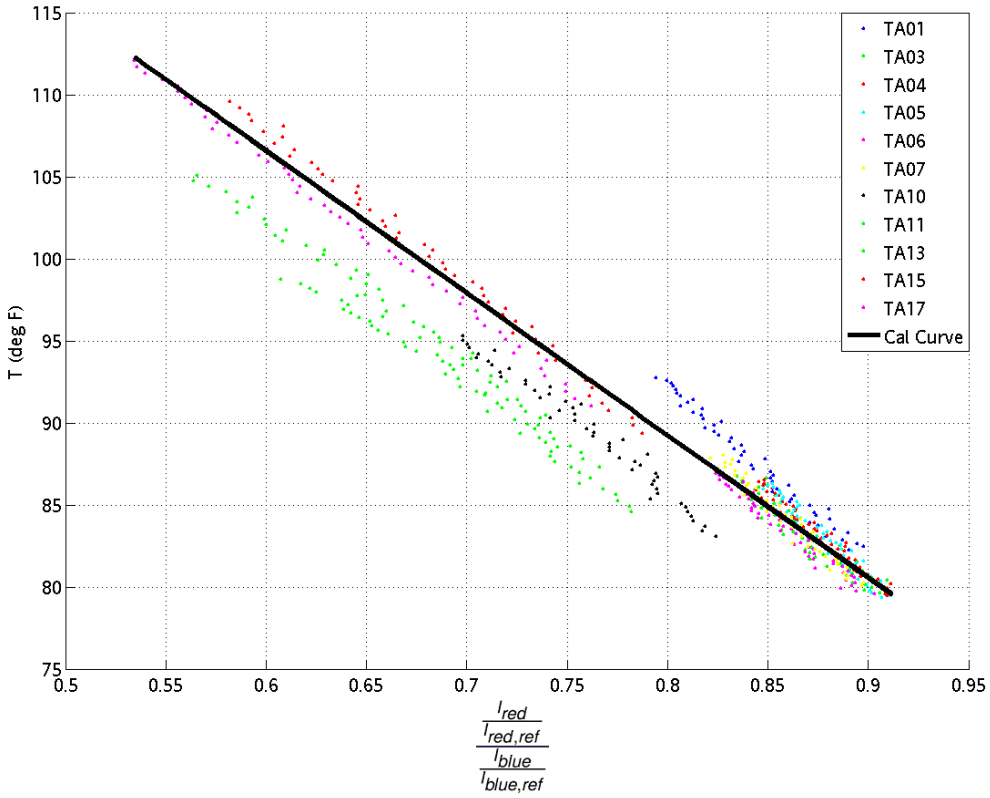

Figure 10. All instrumented locations along a model cross-section for Test Program 2: Run 5 with calibration curve.

Note that the calibration curve, while adequately approximating the behavior of the majority of locations, fails to appropriately describe the behavior of locations TA01, TA10, TA11 and TA13. These locations are said to exhibit "off calibration" behavior. A subset of thermocouple locations is chosen when creating the calibrations rather than the entire set of data because current work has shown that including

locations that deviate significantly from the general trend can have a deleterious effect on the determination of heat transfer results. Discrepancies between the model surface temperature as determined by the calibration curve and actual model surface temperature as recorded by the thermocouple at that location lead to errors in the boundary condition temperature values supplied to the data reduction algorithm which results in errors in the heat transfer results locally at those areas on the model. Observed discrepancies in the heat transfer results determined by TSP and thermocouple data can be on the order of 50% difference for particularly large discrepancies. Further discussion of this phenomenon follows.

2.4: TSP vs. Thermocouple Based Heat Transfer Result Discrepancies

Figure 11 below is an example of the discrepancies observed when comparing the heat transfer results determined from the TSP temperature measurements versus the thermocouple temperature measurements. The plot shows normalized Stanton number versus normalized model location for certain areas on the model. The black squares are the Stanton number results based on the thermocouple data whereas the green asterisks plot the Stanton number results at the same location using TSP data as a basis for the data reduction process. A key goal of this work is to gain insight into the possible root of these discrepancies and to produce alternative data reduction methods or improvements in the existing process to mitigate these discrepancies. Ideally, both the thermocouple and TSP based methods would produce identical heat transfer data at a given location. For most locations on the model, the TSP and

thermocouple based heat transfer results are in good agreement, but there remain areas where discrepancies persist.

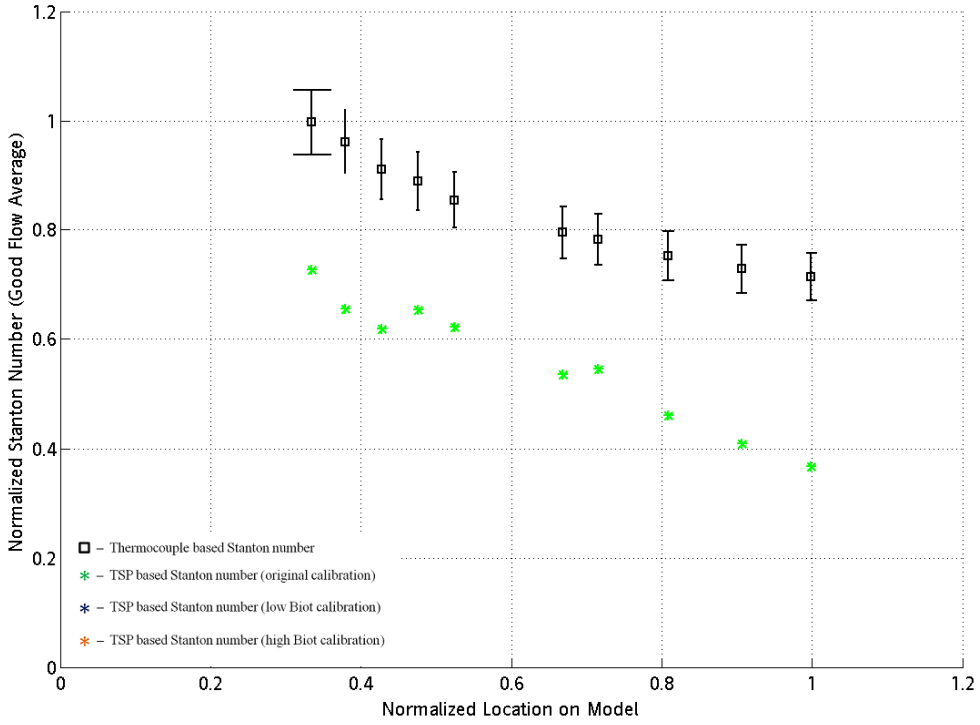

Figure 11. Normalized Stanton number versus normalized model location for Test Program 2: Run 1.

Any calibration using a best fit estimate will incur residual errors as compared to experimental data. However, it was hypothesized that additional errors caused by high local heating rates, thicker areas of coating and non-linear variations in thermophysical properties of the TSP coating with respect to temperature contributed to increases in discrepancies between the two methods. An improved TSP data reduction method would ideally reduce the number and severity of discrepancies

caused by these factors. This hypothesis was driven by the fact that, in general, most discrepancies tended to occur at areas of high heating and involved the TSP method overpredicting heat transfer as compared to the corresponding thermocouple heat transfer result. These discrepancies indicated the possibility of heat storage occurring inside the TSP coating layer. Estimates for the thermal conductivity of the TSP formulation, shown in Section 3.1, have shown that thermal conductivity of the paint decreases as temperature increases. For instance, a temperature rise of 10°F can lead to a thermal conductivity decrease of more than 10%. Heat storage would be most likely in areas of the model that experienced high local heating rates as well as areas with thicker paint layers that provided more thermal resistance than thinner layers. These issues are further exacerbated by non-linear variations in the thermophysical properties of the paint layer with respect to temperature. Note that for areas experiencing low heating rates, temperature rise during a run is smaller than temperature rise at a location exposed to higher heating loads. A larger temperature rise can result in a lower thermal conductivity for the TSP during the course of the run. The lowered thermal conductivity and resulting heat storage could produce the off calibration behavior seen above. An additional problem with heat storage in the coating is the potential to affect the data recorded by the thermocouples underneath the paint layer. A key feature of an ideal TSP system is that heat transfer data is obtained in a non-intrusive manner. Specifically, the combination of emission data and proper data reduction should produce heat transfer results identical to those that the model would experience if the coating were not applied.

Section 3 focuses on the analysis of the tunnel data in pursuit of determining whether the hypotheses described here accurately reflected the physical mechanisms behind the observed discrepancies as well as possible methods of addressing these issues and reducing the number and severity of the observed discrepancies.

Chapter 3: Analysis of Tunnel Data

The set of heat transfer results produced using the TSP measurements in conjunction with the *in situ* calibration was used to analyze and evaluate the data reduction method used at Tunnel 9. Specifically, comparisons between heat transfer results based on TSP measurements were made to heat transfer results obtained by thermocouples instrumented at the same location. The goal of the analysis was to determine what factors influenced the accuracy of the TSP based heat transfer results and to determine ways of improving accuracy in areas where the discrepancy between the results were significant. Data from the instrumented thermocouple locations was analyzed for each run and sorted. Specifically, sorting focused on identifying locations where there was a large observed discrepancy between heat transfer and also highlighting areas of the model that displayed large deviations from the run specific calibration curve as seen in specific locations included in Figure 10. By comparing properties of these sorted subsets against one another, influential parameters could be determined. The parameters recorded in the sorted lists for the locations investigated included: *in situ* calibration based quantitative temperature at the beginning and end of the good flow period of the run, the rate of temperature rise during the good flow period of the run, the thickness of the coating at the given location, thermocouple temperature measurements at the beginning and end of the good flow period of the run, the heating rate and Stanton number at the beginning and end of the good flow period of the run, the average Stanton number throughout the good flow period of the run, and finally, the Biot number at the beginning and end of the run as well as the average Biot number for the entire good flow portion of the run.

Briefly, the Biot number is a measure of the ratio of convective to conductive heating at a particular location. A more in-depth explanation of the Biot number and its use in this work is presented in Section 3.3.

3.1: Estimates of TSP Thermophysical Properties

The set of thermocouple data was used to determine estimates of the TSP thermophysical properties. Measurements of the density and specific heat of the TSP coating were obtained from samples sent to the Thermophysical Properties Research Laboratory (TPRL) Incorporated. Measurements of specific heat with respect to temperature were determined using a differential scanning calorimeter at TPRL. The estimate of the thermal conductivity of the TSP coating was obtained using methods developed in Ref. 4 and compared against measurements of thermal conductivity as obtained by the Air Force Research Laboratory (AFRL). TPRL determined that the coating had a density of 0.0325 lbs. per cubic inch. The specific heat of the coating varied nonlinearly with temperature and is shown in Figure 12 below.

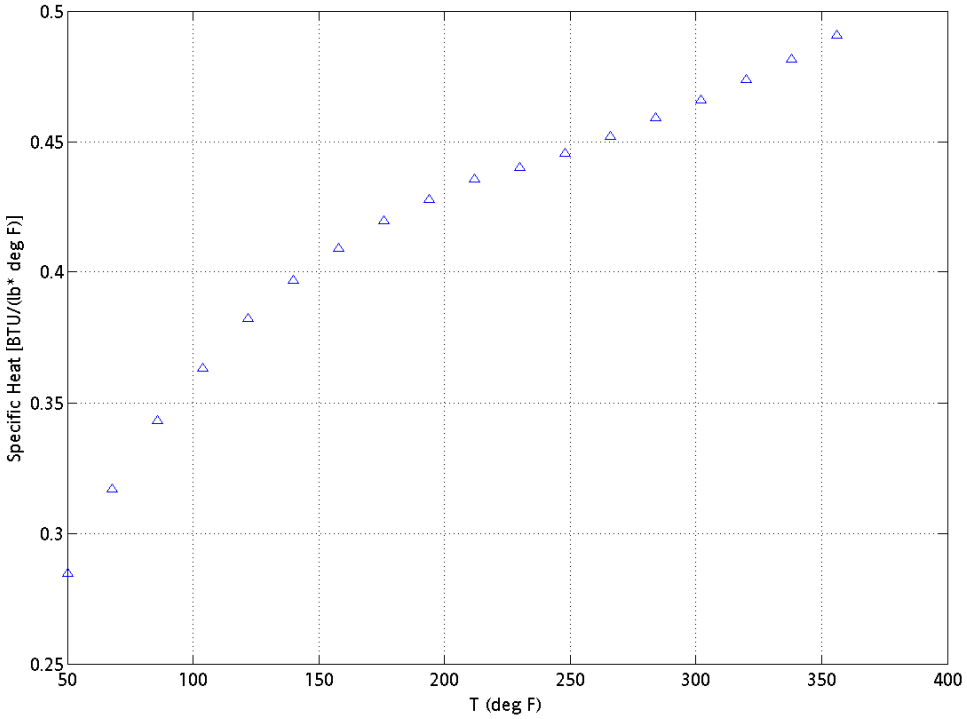

Figure 12. Specific heat of TSP coating versus temperature.

Note that Eqn. 7, repeated here for convenience, provides a solution for k_1, the TSP thermal conductivity, given values of k_2, the thermal conductivity of the model material, nodal temperatures T_1, T_2, and T_3, paint thickness, L, and nodal thickness, Δx.

$$k_1 = k_2 \frac{L}{\Delta x} \frac{(T_2 - T_3)}{(T_1 - T_2)} \tag{7}$$

In this case, the model material is known to be 17-4 PH stainless steel with well-known thermophysical properties. The temperatures T_1 and T_2 are determined directly from the TSP coating emission data and the thermocouple data respectively. Finally, T_3 is determined based on the aforementioned second order, Euler explicit, finite-difference approximation method used to solve the transient 1-D heat equation. The

method allows for the determination of temperature at nodes distributed throughout the depth of the model given the appropriate boundary condition data, which in this case is the thermocouple temperature time history data or T_2. In addition to producing estimates for a two-color TSP formulation rather than the one-color TSP used in Ref. 4, the present work analyzes a larger dataset than the previous work in an effort to more precisely determine the value of the thermal conductivity of the TSP. Specifically, the current work utilized data gathered from 7 tunnel runs and multiple locations on the model for each run to determine the estimate for the thermal conductivity as shown in Figure 13 below. The blue line indicates the estimate of thermal conductivity produced from work carried out in Ref. 4 whereas the red line indicates the estimate of thermal conductivity produced from the current work. The single error bar highlighted in the red line indicates the uncertainty inherent in these estimates, equal to ± 25% of the indicated value. The large uncertainty is mostly due to difficulties in accurately measuring paint thickness at a specific location as mentioned earlier. In addition to the ± 16% uncertainty in the measured paint thickness, the temperature measurements are accurate to within ± 4°F.

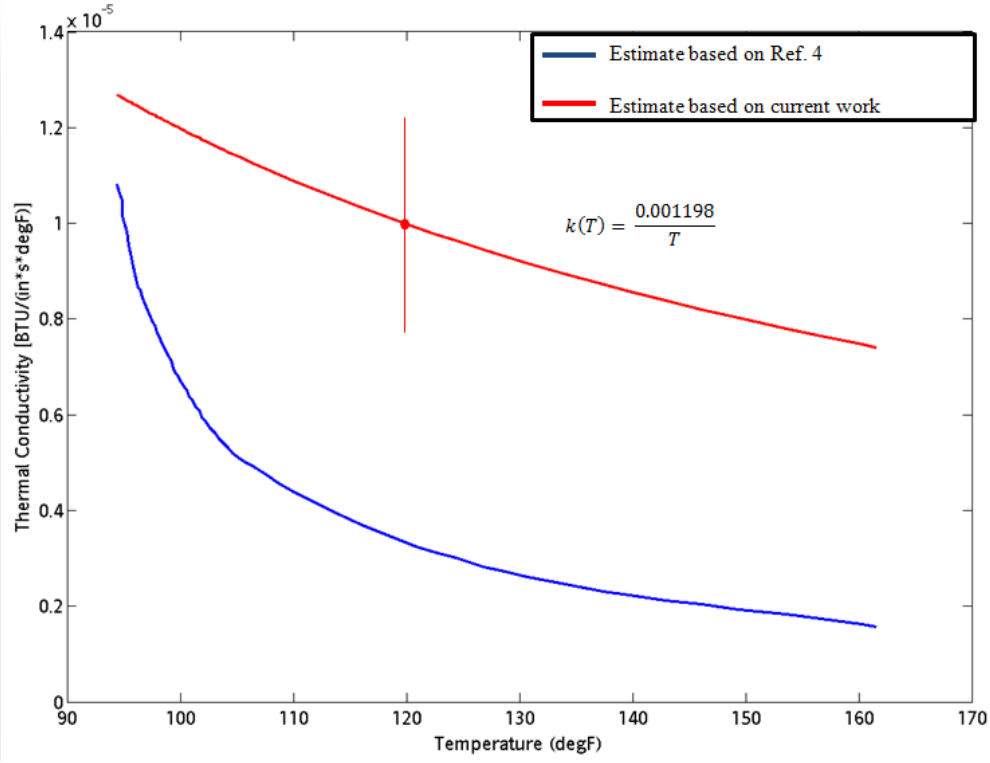

Figure 13. Thermal conductivity estimates for TSP coating. Estimate based on Ref. 4 versus estimate based on current work.

Samples of the TSP coating were also tested at the Air Force Research Lab (AFRL) to determine thermal conductivity over a range of temperatures. Figure 14 below shows a comparison of the AFRL results for various sample thicknesses versus the estimates for thermal conductivity produced in Ref. 4 as well as the estimate produced in the current work. Note that the revised estimate of thermal conductivity produced in this work matches relatively closely with the measurements made by AFRL.

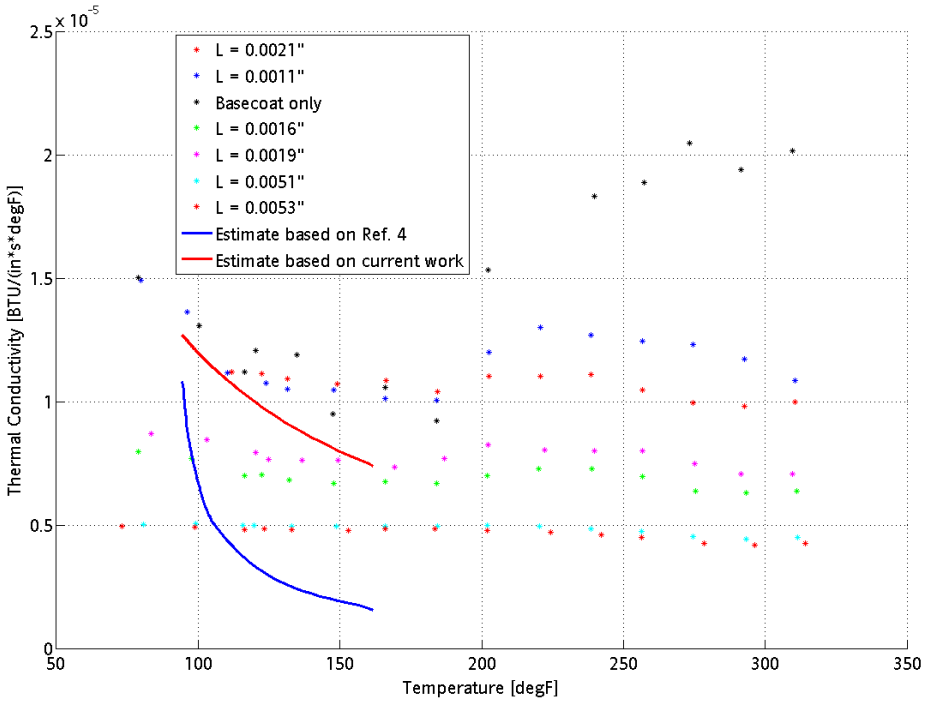

Figure 14. Thermal conductivity estimates for TSP coating. AFRL data versus estimates based on Ref. 4 and current work.

Note here that the spread seen amongst the AFRL measurements is another indicator of the large uncertainty inherent in determining thermal conductivity for the TSP samples. Thermal conductivity is a material property that should not vary with respect to thickness, yet the difficulty involved in making quality samples of a given thickness leads to the large uncertainty in the measured values for conductivity.

3.2: ANSYS Simulations of Paint Behavior

These thermophysical property values for density and specific heat as well as the estimate for thermal conductivity were used in ANSYS, a commercial finite element program, to create a 1-D two layer model to analyze the behavior of the paint

under various simulated loads. The ANSYS model was designed around the nominal characteristics of a typical Tunnel 9 test article, namely, a 0.375 inch steel model wall coated with TSP. Coating thicknesses of 1 mil, 2 mil, 3 mil, 4 mil and 5 mil were tested. Each simulation split the TSP layer into 6 elements per mil and the steel model wall was modeled with 200 elements biased such that elements were thinner near the TSP-steel interface and thicker towards the back wall. This biasing provides higher resolution close to the area of interest. Reference 4 utilized the same mesh parameters for the TSP layer in a similar analysis of paint behavior. An example of the ANSYS schematic for a 1 mil thick TSP layer is shown below in Figure 15.

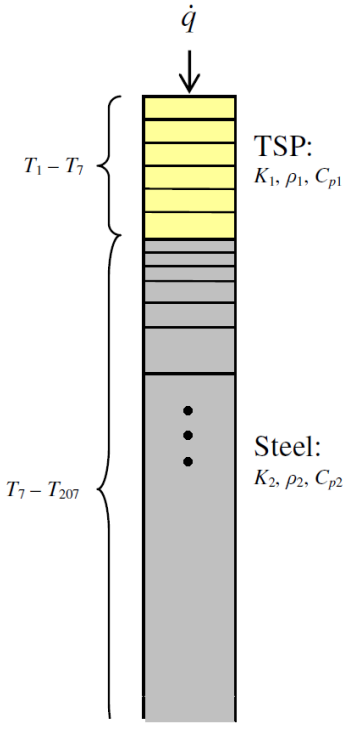

Figure 15. Schematic of ANSYS model of TSP layer and model wall.

Material models were created inside the program for the stainless steel and the TSP coating. The thermophysical properties of the stainless steel test wall are well

known and were entered into the model. Specific heat and density of the TSP coating was inputted based on the values determined by TPRL. The thermal conductivity of the TSP coating was estimated using the technique described in Section 3.1 and applied. A uniform initial temperature of 65°F was applied for the entire model. The heating loads were modeled as a two-part ramp load over a total runtime of 2 seconds to mimic loads seen by the test articles during a typical tunnel run. From 0 – 0.1 seconds, a sharp rise in load corresponding with the startup flow was modeled followed by a ramped heat load corresponding with the good flow period of the run from 0.1 – 2 seconds. An example of the idealized heat load profile used by the simulation is shown in Figure 6 b). Five heating loads were tested, ranging from 5 BTU per ft^2 per second to 30 BTU per ft^2 per second. This corresponded with the range of heat loads seen in the data gathered from multiple tunnel runs. A 0.001 second time step was used to ensure convergence of the finite element model and data was recorded at every 0.002 second interval to be used in time history analysis.

A typical screenshot with the results of the simulations carried out for the 2 mil baseline case with a 10 BTU per ft^2 per second load at t = 1 second is shown below in Figure 16. This specific set of parameters was chosen as the baseline as the typical coating thickness was approximately 2 mils and because 10 BTU per ft^2 per second was a common heat load observed on various areas of the test article.

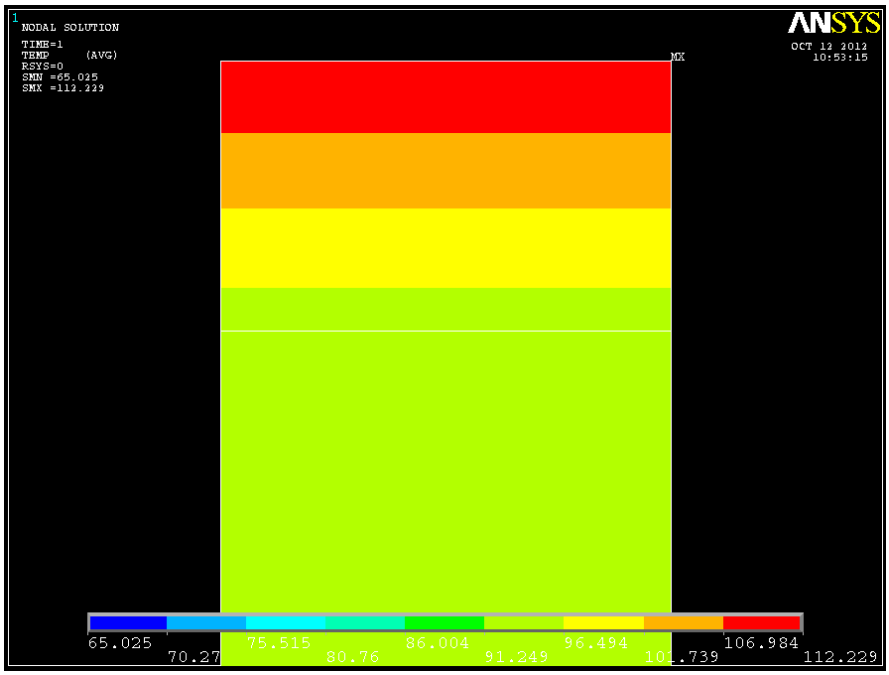

Figure 16. Screenshot of 2 mil TSP coating thickness, 10 BTU per ft^2 per second baseline model at t = 1 second.

3.2.1: Validation of Linear Temperature Gradient Assumption Using Simulated Paint Behavior Models

Ref. 4 used a similar analysis of TSP behavior under simulated loads to examine the appropriateness of the linear temperature gradient assumption used in the *in situ* calibration data reduction method. The current work uses the new property values and estimates of the TSP coating and evaluates the validity of this assumption for the two-color TSP coating used at Tunnel 9. To determine the linearity of the temperature gradient throughout the paint layer, a linear fit was taken from the nodal temperature at the surface of the paint to the nodal temperature at the paint-steel interface for each timestep. The deviation from the idealized linear fit was expressed in terms of an R^2 value for that specific timestep. In the linear case, R^2 can be

determined from the proportion of the total sum of squares that is explained by the regression sum of squares. For example, a true linear temperature gradient would produce an R^2 value equal to 1 when compared in this manner. This R^2 plot was calculated for each simulated load and for all paint thicknesses considered. Figure 17 below shows the R^2 value versus time for 5 different simulations with heat load equal to 10 BTU per ft^2 per second. Note that the typical TSP coating thickness is on the order of 2 mils and that the 10 BTU per ft^2 per second value is a commonly observed heat load seen on the test article. The temperature gradient inside the paint layer has an R^2 value that is nearly one throughout the entire run for this set of simulations.

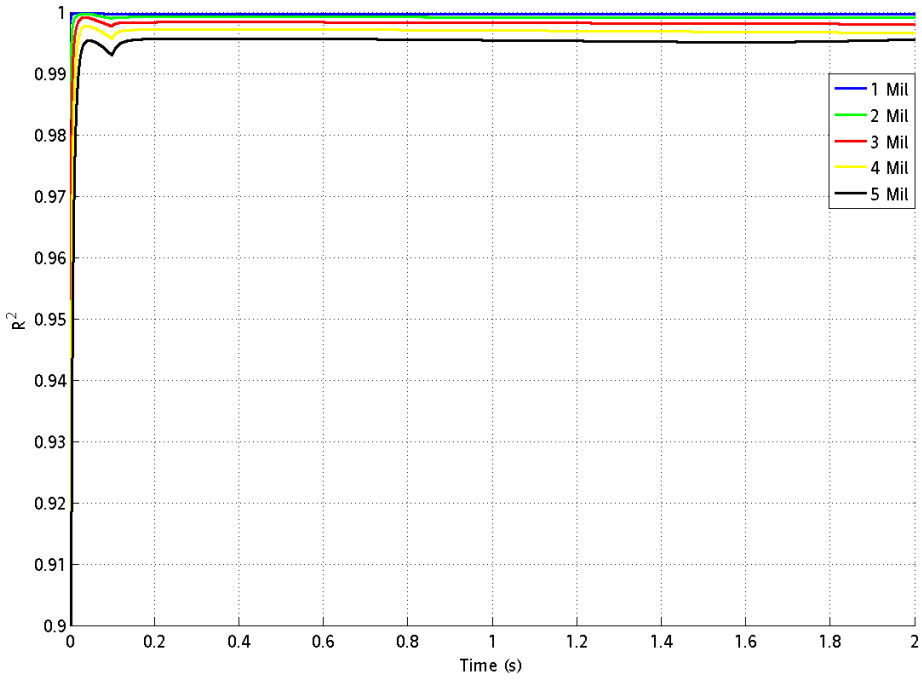

Figure 17. R^2 value of temperature gradient in TSP layer versus time. ANSYS simulation with 1-5 mil TSP layer subjected to 10 BTU per ft^2 per second load.

Figure 18 below shows the R^2 value at each timestep for the simulated load of 30 BTU per ft^2 per second with a steel model covered with a 5 mil thick paint layer. This simulated load and paint thickness are larger than any in the set of tunnel data analyzed. However, it is useful for validation purposes in that the R^2 value even at this extreme thickness and heat load is essentially 1 for the entire good flow period (0.1 seconds to 2 seconds).

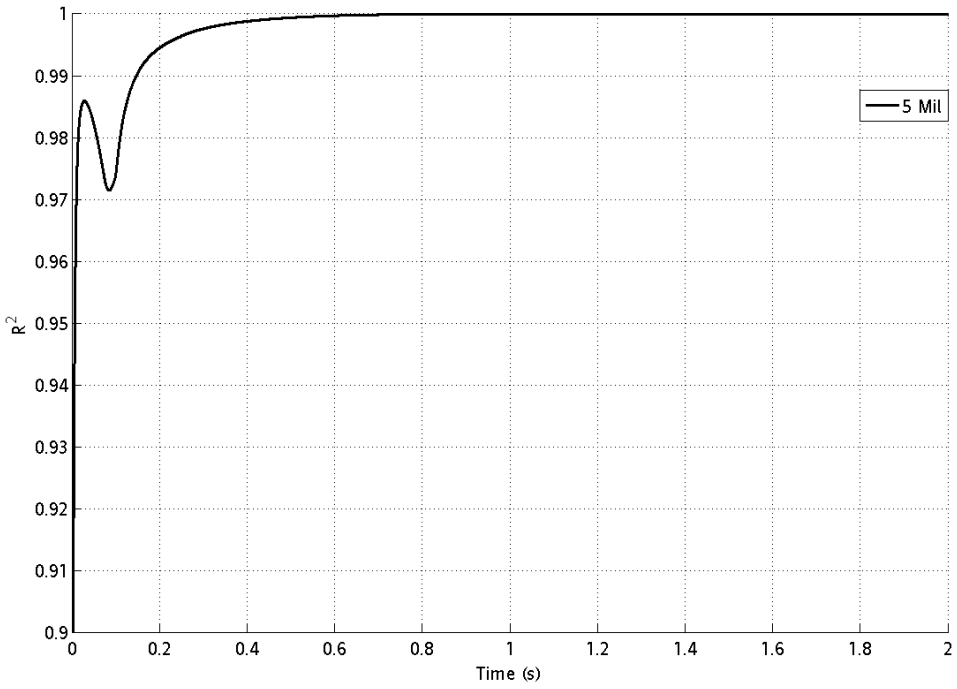

Figure 18. R^2 value of temperature gradient in TSP layer versus time. ANSYS simulation with 5 mil TSP layer subjected to 30 BTU per ft^2 per second load.

This indicates that based on the estimated thermophysical properties, the linear temperature gradient assumption is a good approximation of the actual gradient within the paint layer based on simulated results. R^2 values for lower heating loads

and thinner paint layers are even closer to 1 at each timestep. Note that the simulated values for the temperature gradient are strongly dependent on the estimated thermophysical properties. For instance, a constant value estimate for thermal conductivity results in temperature gradients that are always linear.

3.2.2: Variation in Paint Thermophysical Properties and Thickness and their Effect on Heat Transfer Results

The ANSYS simulations were also used to perform a sensitivity analysis of the percent error in heat transfer calculations caused by perturbations in paint thermophysical properties and paint thickness. Additional insight into the physical mechanisms affecting the data reduction process can be determined by identifying the most sensitive factors involved. A baseline simulation of a 2 mil paint coating thickness with a 10 BTU per ft^2 per second load profile was chosen. The density, specific heat and thermal conductivity were each varied independently ± 5, 10 and 20%. This variation was done to mimic the range of uncertainty observed in the estimated thermal conductivity measurements. The paint coating thickness was varied ± 8.33 and 16.66% – equivalent to ± 1 and 2 elements, respectively, in the finite element model for the TSP layer. Again, this variation was set by the uncertainty in the measured average sectional paint thickness values. In sum, a total of 22 simulations with independent paint thermophysical property or paint thickness variations as compared to the baseline case were analyzed. The heat transfer values of the perturbed models were compared against the baseline case to examine the percent error in heat transfer results. The results are shown in Table 1 below. Note that large

variations in the specific heat and density property values do not cause appreciably large deviations from the baseline heat transfer results; however, the data reduction process is far more sensitive to variations in the thermal conductivity or paint coating thickness values.

Table 1: Sensitivity analysis of paint properties and thickness

	Percent Error in Heat Transfer Results Caused by Perturbation in:			
Perturbation	Density	Specific Heat	Conductivity	Thickness
+20%	0.020%	0.021%	6.45%	-5.71%
+10%	0.014%	0.014%	3.42%	-2.95%
+5%	0.011%	0.011%	1.76%	---
-5%	0.004%	0.004%	-1.88%	---
-10%	0.001%	0.001%	-3.89%	3.12%
-20%	0.005%	0.005%	-8.30%	6.46%

The results of the sensitivity analysis were used to inform the choice of parameters investigated in the evaluation of the tunnel data. Specifically, a non-dimensional analysis of the tunnel data was carried out in an effort to better understand the limits of and improve the current data reduction method.

3.3: Non-Dimensional Analysis

A variety of non-dimensional parameters were investigated including Stanton number and Fourier number amongst others, but the Biot number and Reynolds number were the most useful non-dimensional parameters used in the current work.

The Reynolds number is a commonly used engineering figure describing the ratio of fluid inertial and viscous forces. The equation for the Reynolds number is shown in Eqn. 13 where ρ is the density of the fluid, U is the flow velocity, L_c is a characteristic length and μ is the viscosity of the fluid. Generally speaking, the Reynolds number is used in wind tunnel testing as a condition of flow similarity and for empirical determinations to identify areas of flow transition and turbulence on a test article.

$$Re = \frac{\rho U L_c}{\mu} \tag{13}$$

The Biot number is a ratio of the convective versus conductive heating for a given solid. Eqn. 14 below shows the equation used to determine the Biot number where h is the convective heat transfer coefficient, L_c is a characteristic length – in this case, the paint coating thickness – and k is the thermal conductivity of the TSP coating.

$$Bi = \frac{hL_c}{k} \tag{14}$$

The Biot number is a useful dimensionless figure used in the evaluation of the tunnel data as it incorporates the parameters identified as being most influential to the heat transfer results based on the sensitivity analysis performed in Section 3.2.2. In general, the smaller the Biot number, the more uniform the temperature field inside the body itself. Note that the convective heat transfer coefficient can be defined as seen in Eqn. 15 where St is the Stanton number, C_p is the specific heat of the working fluid, ρ_∞ is the freestream density of the working fluid and U_∞ is the freestream flow velocity.[44]

$$h = St * C_p * \rho_\infty * U_\infty \tag{15}$$

This treatment for determining h relies on an empirical relationship determined for laminar hypersonic flow over a flat plate at constant pressure and temperature, but has

been used in other recent works to approximate the convective heat transfer coefficient.[45] Therefore, using Eqn. 15 and the heat transfer results based on the set of thermocouple tunnel data, it is possible to determine the convective heat transfer coefficient for every instrumented location on the model. The temperature dependent estimate of thermal conductivity shown in Section 3.1 is used to approximate TSP thermal conductivity. Finally, the paint coating thickness must be known in addition to the convective heat transfer coefficient and the thermal conductivity of the TSP coating to calculate the Biot number. Note that the thickness was measured in two ways, with a magnetic induction probe and also with micrometer measurements of peeled paint strips. Probe measurements were taken at various locations on the test article and averaged to provide an average coating thickness for a particular section of the model. This was done because the magnetic induction probe measurements were sensitive to test article curvature and embedded instrumentation. The micrometer measurements were not affected by these factors and better approximated coating thickness at specific locations, particularly those areas directly above instrumented thermocouples. For that reason, these micrometer based thickness measurements were used to determine Biot numbers for instrumented locations rather than the average sectional coating thickness determined using the magnetic induction probe.

Each unique tunnel condition required a specific set of criteria to enable sorting of the tunnel data. For example, when determining the on calibration versus off calibration locations for a given run, all locations of interest were plotted with the calibration curve determined for that run. In other words, the entire set of thermocouple and TSP data was plotted on a temperature vs. ratio of ratio plot.

Generally, the data were clustered such that a specific calibration curve could be subjectively determined using engineering judgment. The locations were then sorted into on calibration or off calibration classifications relative to the other locations investigated and the deviation from the calibration curve. Similarly, the heat transfer discrepancy classifications were determined relative to the average discrepancy of the investigated locations for a specific run.

The sorted data sets were analyzed using the Biot number and Reynolds number values to determine if a trend existed that would allow tunnel data to be classified without subjective and labor-intensive manual sorting techniques. Figure 19 below depicts the average Biot number over the course of a run versus the Reynolds number per foot in millions. The red data points represent tunnel data that has been classified as off calibration for any given run and the green data points represent tunnel data that has been classified as on calibration. The green trend line is a linear best fit to the on calibration data points. Note that most of the off calibration data points are on one side of the green trend line. Specifically, higher Biot numbers than those predicted by the trend line at a given Reynolds number per foot are more susceptible to being classified as off calibration. In that sense, the trend line equation can be used as a rough indicator of areas that may require closer scrutiny during the data reduction process and also as an indicator of areas where the current data reduction process has acceptable error in the heat transfer results.

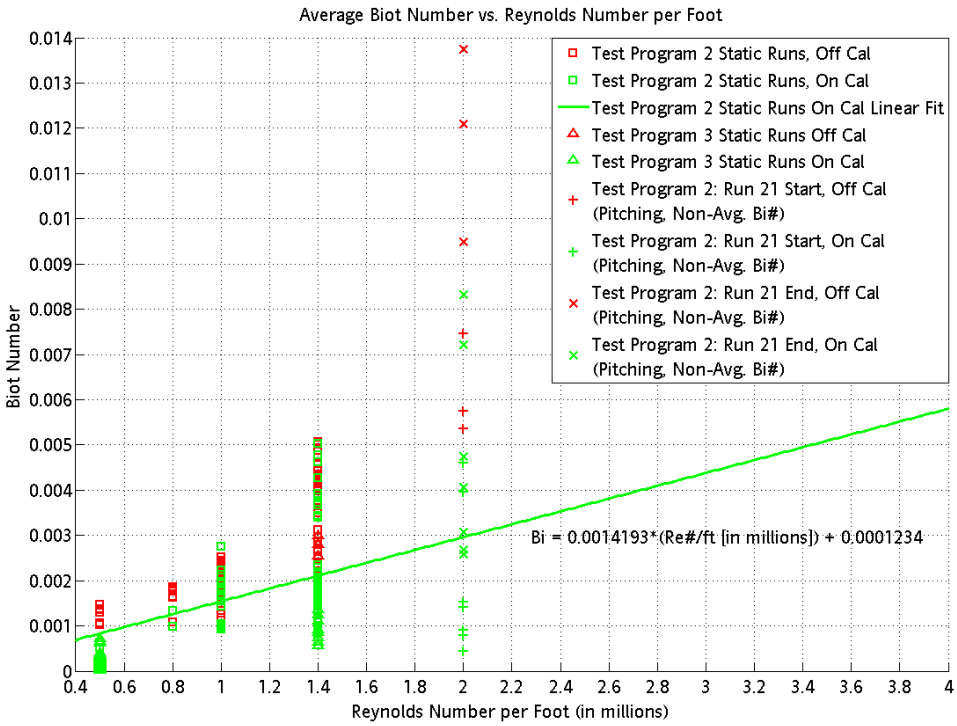

Figure 19. Average Biot number versus Reynolds number per foot.

There was significant overlap between the off calibration sorted dataset and the locations showing large discrepancies between TSP and thermocouple based heat transfer results. Therefore, it was postulated that a calibration method focusing on the high Biot number dataset could reduce the discrepancies observed in the heat transfer results.

3.4: Two Curve Calibration Data Reduction

One proposed solution to the observed problem is a two calibration data reduction process. To perform the two calibration data reduction, the existing data reduction procedure was first performed on the dataset. Namely, the *in situ* calibration was determined subjectively as before and an estimate of the average Biot number for

a given location during the good flow portion of the run was determined. Using the Biot number trend line equation shown in Figure 19, the data was sorted into high Biot and low Biot number sets depending on whether the Biot number for the location was greater than or less than the trend line value for the Biot number at the given Reynolds number run condition. A second pass of the *in situ* calibration was performed with two separate calibration curves. One curve was determined from the low Biot number location data and the other was determined from the high Biot number location data. The low Biot calibration curve was used in the data reduction process for the low Biot number locations and the high Biot calibration curve was used for reducing the high Biot number locations. To determine whether the secondary calibration improved the heat transfer results or not, the difference from the thermocouple based heat transfer results was calculated for both the original and two calibration data reduction methods. The discrepancy was determined by Eqn. 16 below:

$$Discrepancy = \frac{St_{TSP} - St_{TC}}{St_{TC}} \tag{16}$$

where St_{TSP} is the Stanton number as determined using the TSP data and St_{TC} is the Stanton number as determined by the thermocouple data. The average discrepancy percentage was determined by calculating the discrepancy for each data sample taken during the course of the run and averaging over the good flow period. A reduction in this average discrepancy when using the two calibration method to determine St_{TSP} instead of the original calibration method would indicate that the two calibration method improved the TSP data reduction process. This improvement would entail producing heat transfer results more in line with those determined using the standard

thermocouple based data reduction process. Furthermore, the maximum discrepancy was also noted for the entire good flow period. Again, a reduction in the maximum discrepancy would indicate that the two calibration method was producing results more similar to the results produced by the standard thermocouple based method.

Chapter 4: Results and Discussion

4.1: Example Two Curve Calibration Process

The two calibration data reduction method was used in an attempt to lower the frequency and severity of observed discrepancies seen between heat transfer results determined from the thermocouple and TSP data respectively. An example of these discrepancies was shown in Figure 11 in Section 2.4. An example of the two calibration process and the discrepancy reduction achieved using the two calibration data reduction method for Test Program 2: Run 1 is shown below.

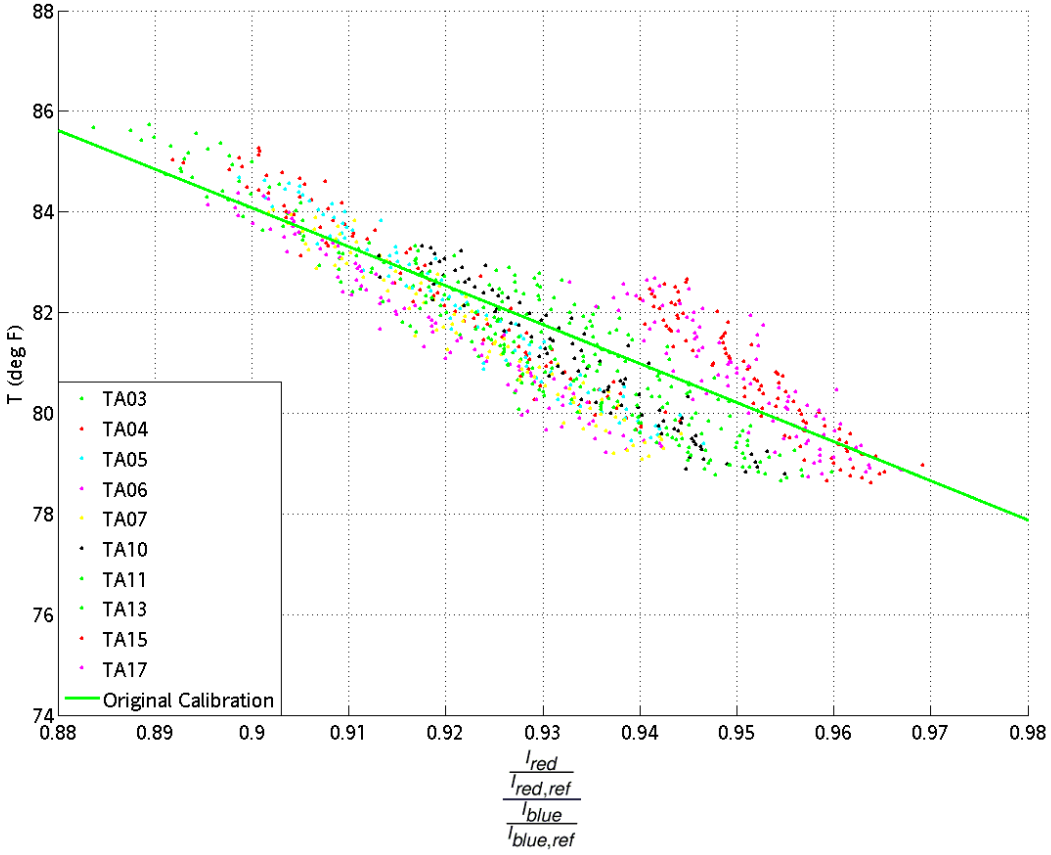

Figure 20. Original calibration for Test Program 2: Run 1.

Figure 20 shows the original calibration for the given run determined subjectively based on trends observed in the data. Estimates of the Biot number at each thermocouple location are determined using thickness data, heat transfer results based on the original calibration or based on thermocouple data if available and the estimate of thermal conductivity for the TSP. Using the Biot trend line equation seen in Figure 19, the locations are sorted into high Biot and low Biot sets. The data reduction process is redone using two calibration curves, one each for the low Biot and high Biot sets. Figure 21 shows the temperature versus ratio of ratios plot with all three calibration curves for Test Program 2: Run 1. Note that the original calibration curve is green, the low Biot calibration curve is in blue and the high Biot calibration curve is in orange. Finally, the data reduction process is carried out using the low Biot calibration for the low Biot data set and using the high Biot calibration for the high Biot data set.

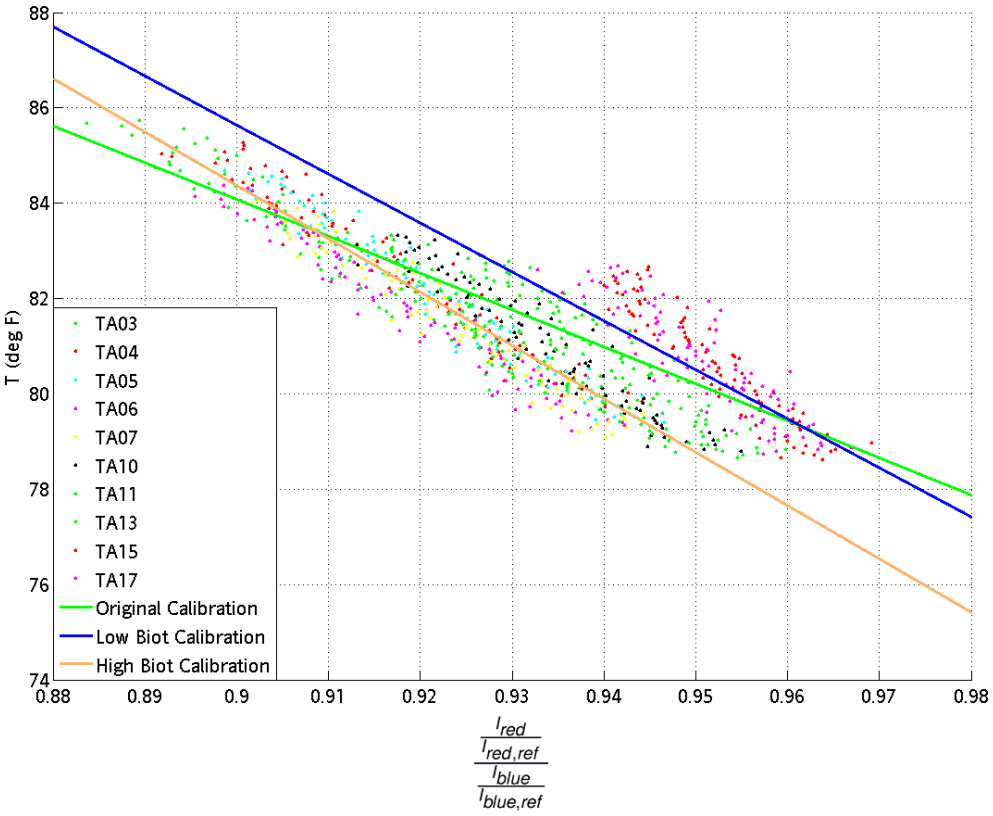

Figure 21. Test Program 2: Run 1. Original, low Biot and high Biot calibration curves.

4.2: Two Curve Calibration Results

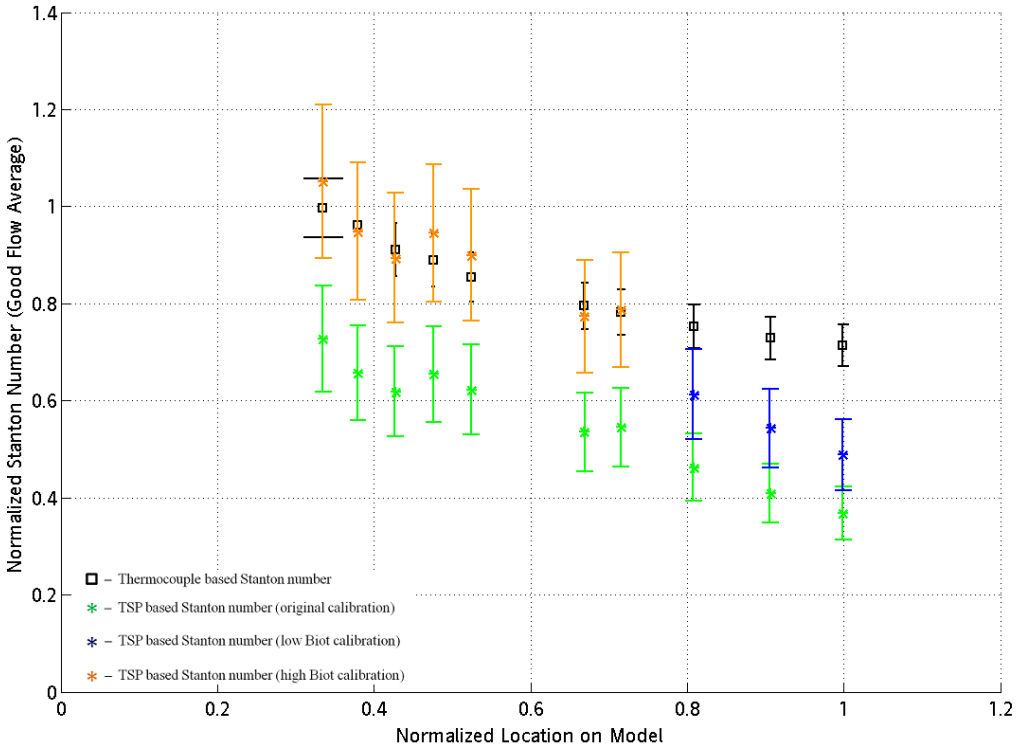

Figure 22. Normalized Stanton number versus normalized model location for Test Program 2: Run 1.

For each frame captured by the camera during the run, a plot showing the Stanton number versus the model location can be plotted. For non-pitching runs, an average Stanton number value for the good flow period is an important measure of aerodynamic heating as well. Note that in Figure 22, the TSP based heat transfer results using the original calibration are shown as green asterisks, the results using the low Biot calibration are shown as blue asterisks and finally the results using the high Biot calibration are shown as orange asterisks. The black squares are the thermocouple based heat transfer results with corresponding ± 6% error. In this case,

there is a clear reduction in the discrepancy between the TSP and thermocouple based heat transfer results when the two calibration data reduction method is used.

Other examples seen below in Figure 23 to Figure 26 depict normalized Stanton number versus model location for selected runs. For these runs, the two calibration data reduction method clearly lowers the discrepancy between the thermocouple and TSP based heat transfer results.

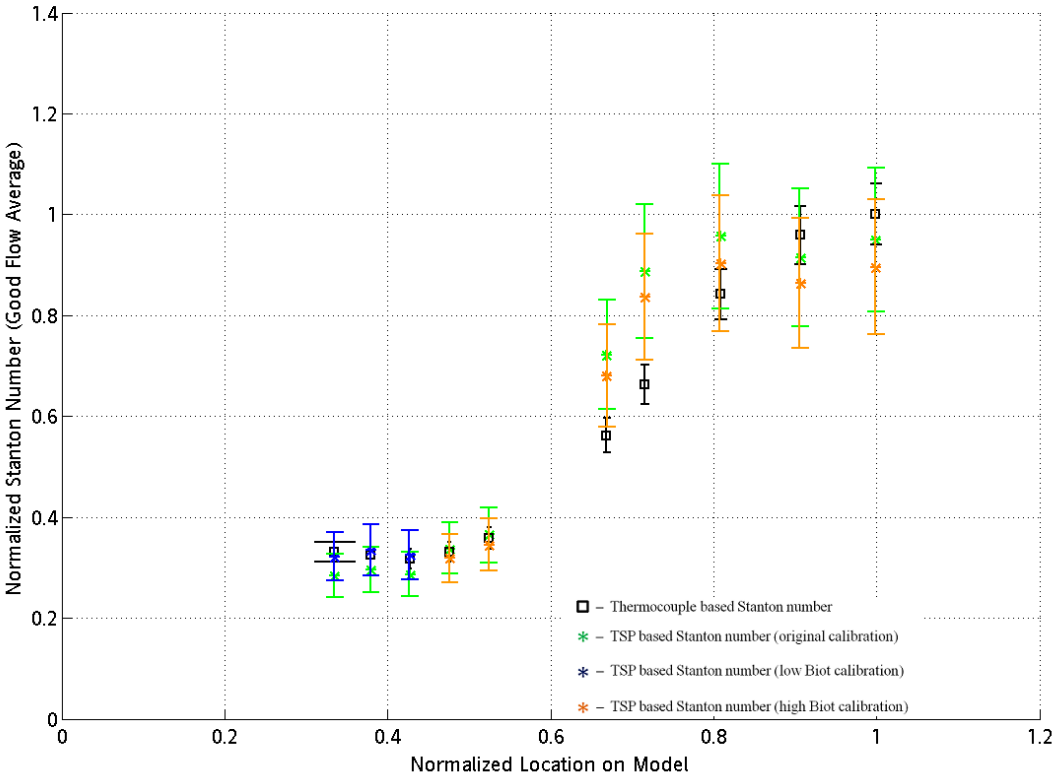

Figure 23. Normalized Stanton number versus normalized model location for Test Program 2: Run 2.

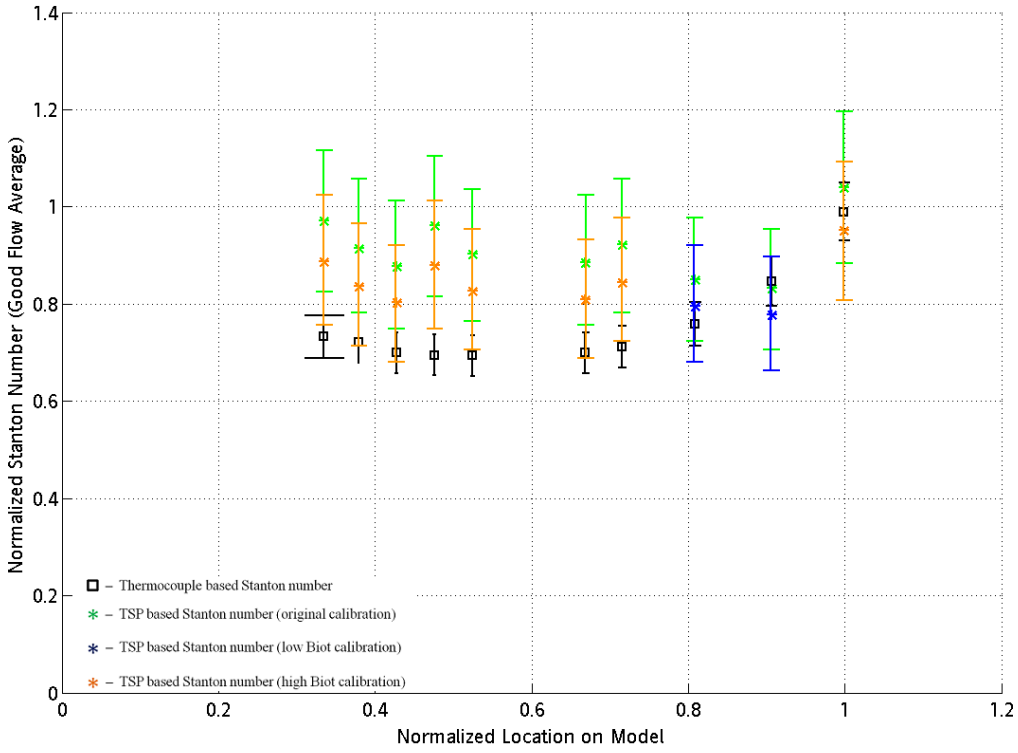

Figure 24. Normalized Stanton number versus normalized model location for Test Program 2: Run 4.

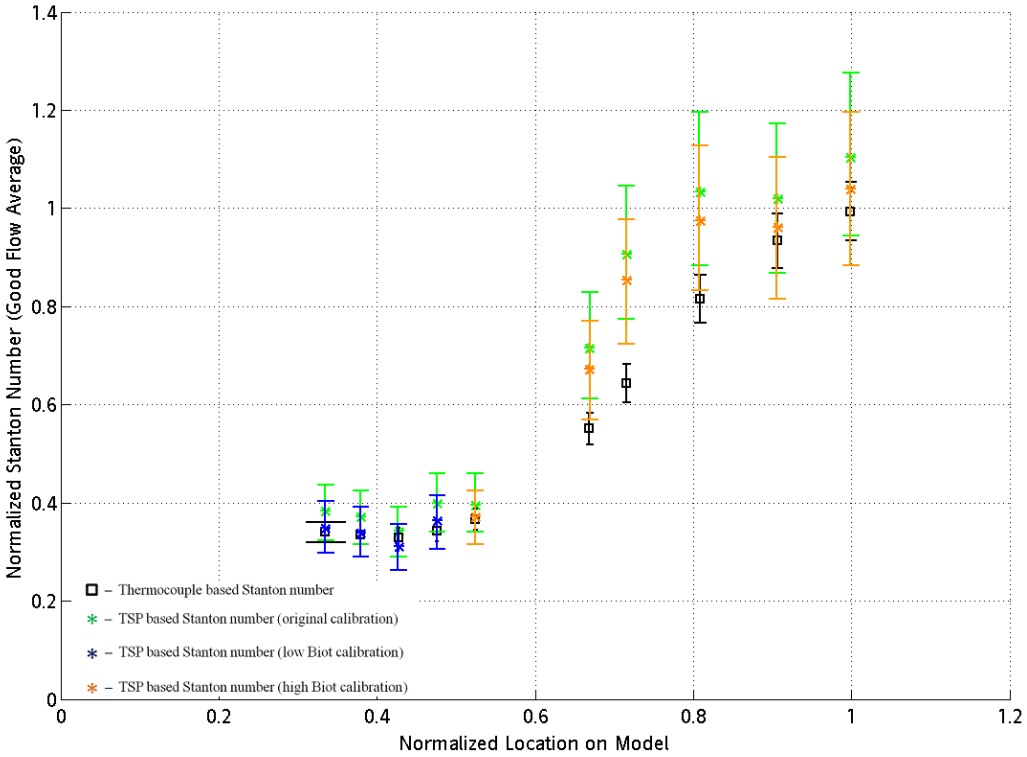

Figure 25. Normalized Stanton number versus normalized model location for Test Program 2: Run 13.

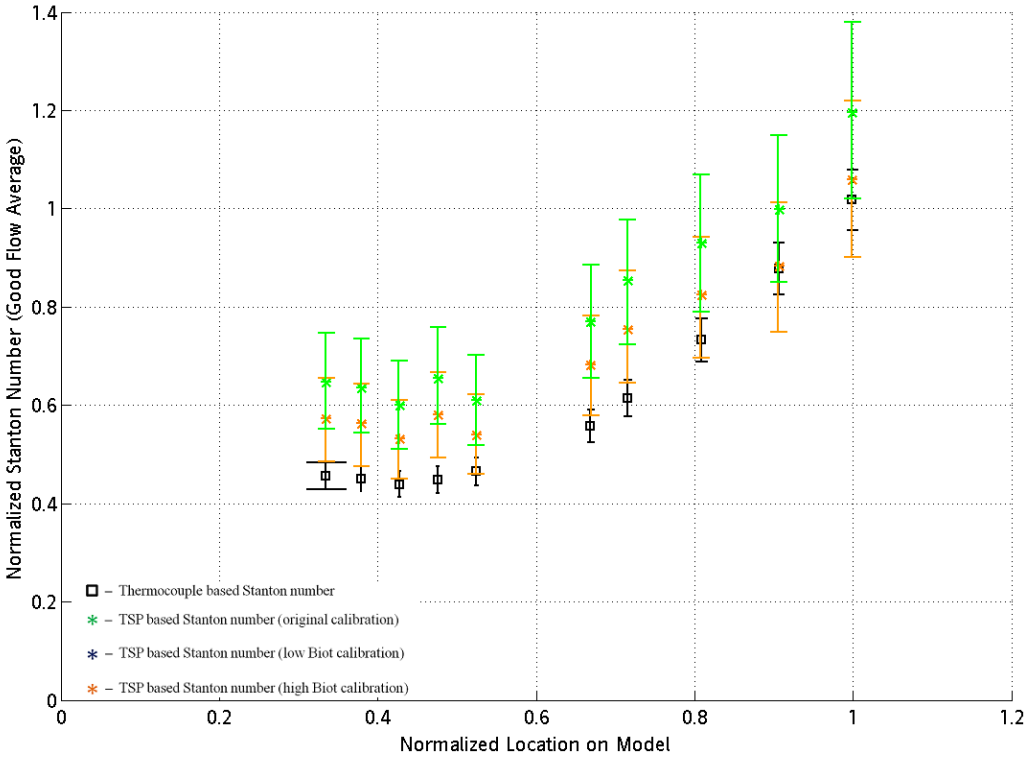

Figure 26. Normalized Stanton number versus normalized model location for Test Program 2: Run 14.

This method is not a cure-all, however, as there remain runs where the two calibration data reduction method actually exacerbates existing discrepancies rather than lowering them. Figure 27 is an example of such a run.

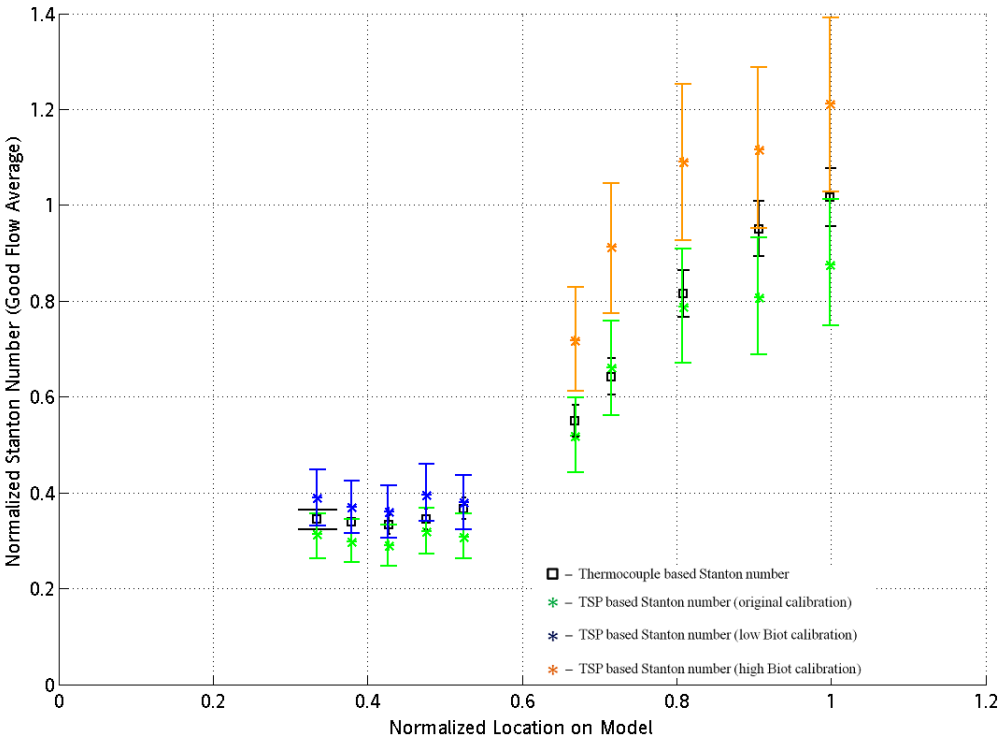

Figure 27. Normalized Stanton number versus normalized model location for Test Program 2: Run 20.

Here, the two calibration method results in more severe discrepancies between the thermocouple and TSP based heat transfer results at all locations of interest. At the present time, research is ongoing into determining the cause of this phenomenon.

Figure 28 below shows the Stanton number results using the original calibration, the high Biot calibration, and results obtained by using a more restrictive calibration based on a subset of the high Biot locations.

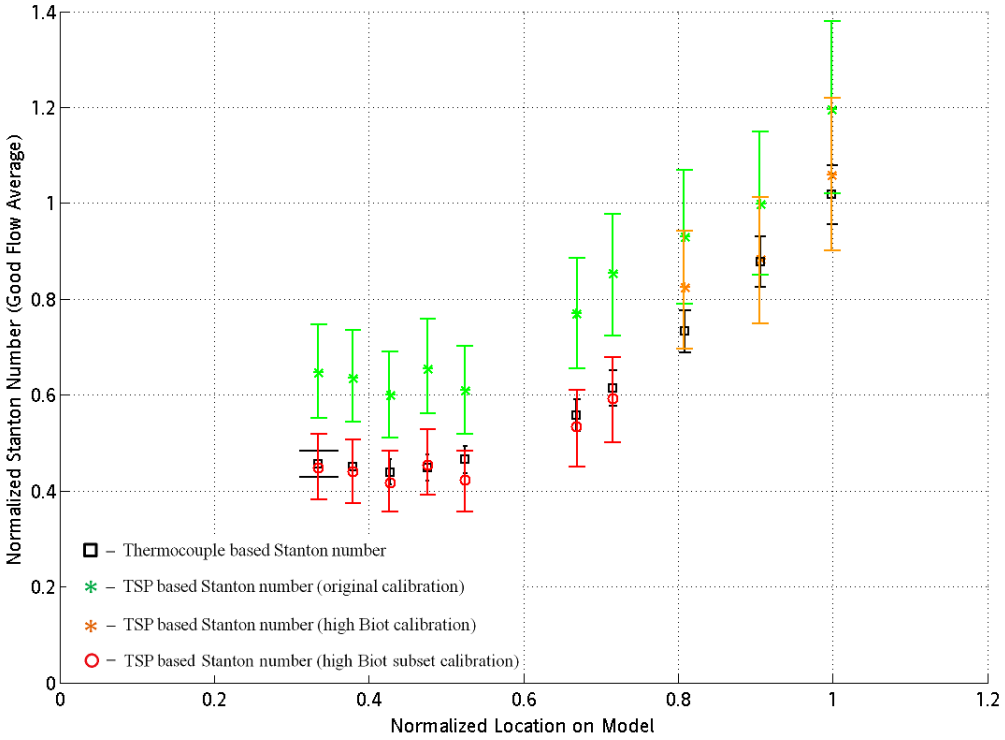

Figure 28. Normalized Stanton number versus normalized model location for Test Program 2: Run 14. Original, high Biot calibration and high Biot subset calibration results.

The more restrictive calibration is applied to normalized locations 0.35 to 0.7 and the resultant Stanton number values for these locations more closely approximate the standard thermocouple based Stanton number results. The combination of the two high Biot calibrations produces results that are dramatically improved from those obtained using the original calibration.

Table 2: Average discrepancy percentage using single calibration method versus average discrepancy percentage using two calibration method for all locations

Test Program 2 Run Number	Initial Discrepancy % Average of All Locations	Post Two Calibration Discrepancy % Average of All Locations
1	29.47	5.95
2	20.08	26.91
3	35.95	46.83
4	36.11	17.74
5	23.87	3.49
6	23.37	34.23
7	9.83	59.68
8	18.95	30.91
9	20.54	14.80
10	7.35	20.13
11	23.29	136.93
12	18.46	101.10
13	21.68	15.43
14	53.18	23.96
15	39.26	52.39
16	17.79	74.22
17	20.00	39.34
18	14.34	15.31
19	28.07	11.96
20	6.39	161.31

Table 3: Average discrepancy percentage using single calibration method versus average discrepancy percentage using two calibration method for high Biot locations only

Test Program 2 Run Number	Initial Discrepancy % High Biot Locations Only	Post Two Calibration Discrepancy % High Biot Locations Only
1	25.00	8.09
2	22.18	15.91
3	33.51	40.84
4	40.69	29.09
5	23.87	7.72
6	n/a	n/a
7	13.88	28.24
8	20.36	14.88
9	30.26	43.33
10	10.06	24.96
11	3.28	11.61
12	14.95	39.29
13	22.12	15.22
14	53.18	35.88
15	41.49	38.00
16	17.79	34.25
17	23.32	36.14
18	14.76	12.56
19	30.45	16.76
20	7.24	33.79

Table 4: Average discrepancy percentage using single calibration method versus average discrepancy percentage using two calibration method for off calibration locations only

Test Program 2 Run Number	Initial Discrepancy % Off Calibration Locations Only	Post Two Calibration Discrepancy % Off Calibration Locations Only
1	24.26	8.99
2	31.35	24.04
3	40.19	45.23
4	44.48	32.37
5	35.68	11.65
6	27.40	32.44
7	20.52	35.99
8	21.72	16.27
9	28.92	35.03
10	12.09	10.66
11	6.42	22.49
12	17.16	41.96
13	26.99	19.75
14	61.25	43.04
15	39.98	42.53
16	11.31	24.02
17	23.32	36.14
18	15.19	13.48
19	29.22	18.90
20	7.87	32.79

Table 5: Average discrepancy percentage using single calibration method versus average discrepancy percentage using two calibration method for low Biot locations only

Test Program 2 Run Number	Initial Discrepancy % Low Biot Locations Only	Post Two Calibration Discrepancy % Low Biot Locations Only
1	39.90	20.60
2	15.20	28.93
3	n/a	n/a
4	17.80	11.33
5	n/a	n/a
6	23.37	28.30
7	5.77	11.97
8	6.25	23.52
9	16.37	4.32
10	7.05	6.67
11	25.51	56.51
12	21.97	28.78
13	21.01	10.36
14	n/a	n/a
15	30.37	53.28
16	n/a	n/a
17	16.68	16.68
18	10.58	22.53
19	24.50	18.73
20	5.54	19.62

Table 6: Average discrepancy percentage using single calibration method versus average discrepancy percentage using two calibration method for on calibration locations only

Test Program 2 Run Number	Initial Discrepancy % On Calibration Locations Only	Post Two Calibration Discrepancy % On Calibration Locations Only
1	34.68	14.70
2	15.26	18.00
3	26.06	30.58
4	16.57	9.61
5	18.81	6.03
6	13.98	18.64
7	5.24	13.30
8	12.47	14.53
9	14.95	3.35
10	4.18	7.06
11	30.52	64.67
12	19.33	28.76
13	18.13	8.96
14	34.35	19.20
15	38.79	40.08
16	20.57	38.63
17	16.68	16.68
18	13.98	13.59
19	17.71	5.37
20	5.41	22.65

Twenty tunnel runs were analyzed using both the original single calibration data reduction method and the two calibration data reduction method. The off calibration and high Biot value locations were of special concern because these locations tended to experience the most drastic discrepancies seen during the tunnel runs. For the twenty runs in question, the average discrepancy value of all off calibration locations using the original data reduction method was 26% as compared to 19% for the on calibration locations. The average discrepancy value of all high Biot locations using the original data reduction method was 24% as compared to 18% for the low Biot locations. Note that it was hypothesized that additional errors caused by high local heating rates, thicker areas of coating and non-linear variations in thermophysical properties of the TSP coating with respect to temperature contributed

to increases in discrepancies between the two methods. This indicates that, in accordance with the hypothesis, off calibration and high Biot locations tended to have more severe discrepancies between the TSP and thermocouple based heat transfer results. Of the twenty analyzed runs, twelve runs showed improvement in terms of lower discrepancy values between heat transfer results based on thermocouple versus TSP data by using the two calibration method. Specifically, seven out of twenty runs showed an overall improvement when comparing average discrepancy values for the original and for the two calibration data reduction method. For the seven runs where this type of improvement was seen, the average discrepancy was lowered from 30% to 13%. When investigating only the locations determined as off calibration, ten out of twenty runs showed improved discrepancy values when using the two calibration method. For these ten runs, the average off calibration location discrepancy value was reduced from 30% to 20%. Finally, when focusing only on the locations identified as having a Biot value higher than the Biot value based on the trend line seen in Section 3.3, ten out of twenty runs showed an improvement in average discrepancy value when using the two calibration method. Specifically for these runs, average discrepancy was lowered from 29% using the original calibration to 19% using the two calibration method. Again, the two calibration method does not completely mitigate all discrepancies seen in the heat transfer results. However, it does improve upon the current method by allowing for the capability to reduce observed discrepancies and also by producing a non-subjective method for determining calibrations for use in the data reduction process.

Chapter 5: Conclusions and Future Work

5.1: Summary

A data reduction method for a global quantitative intensity-based two-color TSP heat transfer measurement system in use at AEDC Hypervelocity Wind Tunnel 9 was evaluated for a series of tunnel runs on a generic hypersonic waverider model. In general, the method performed well in comparison to the standard pre-existing heat transfer measurement system in use at Tunnel 9 which relied on thermocouple sensor data at specific locations on the model. However, some areas of the model showed discrepancies between the heat transfer results determined from the thermocouple based measurements as compared to results determined from the TSP measurement system. It was hypothesized that additional errors caused by high local heating rates, thicker areas of coating and non-linear variations in thermophysical properties of the TSP coating with respect to temperature contributed to increases in discrepancies between the two methods. A more accurate measure of TSP thermophysical properties was determined. Where measurements were not feasible, more accurate estimates of these properties were determined. Similar to previous work done on a prior iteration of the TSP measurement system in use at Tunnel 9, ANSYS finite element modeling software was used to analyze and validate assumptions made in the data reduction approach. Furthermore, ANSYS simulations using the improved thermophysical property measures and estimates were used to perform a sensitivity analysis to determine which perturbed factors contributed most to error in heat transfer results. Based on this analysis, a dimensionless parameter incorporating these

factors, called the Biot number, was used as a basis for a novel two calibration data reduction process in an effort to reduce the severity of the observed discrepancies. While the two calibration data reduction process did not mitigate all observed discrepancies, a reduction in the discrepancy was seen in a majority of the analyzed runs. The reduced discrepancy using the new method lends credence to the proposed hypothesis of high local heating, thicker coating areas and non-linear variations in thermophysical properties leading to additional errors in the data reduction process. Furthermore, the reduction in discrepancy demonstrates that the new data reduction process has the ability to provide improved TSP based heat transfer results. Additional discrepancy mitigation based on a general multiple calibration method, as seen in Figure 28, is possible given continuing research into determining more objective metrics to choose distinct calibration data sets. Ultimately, using a specifically tuned calibration for a given location on the model should allow for minimal discrepancy between the TSP and thermocouple based heat transfer results and more accurate local heat transfer rate measurements even in complex flow fields.

5.2: Use of the Two Calibration Data Reduction Method

The two calibration data reduction method is based on the hypothesis that low Biot and high Biot areas of the test article produce differing calibration curves as seen on the temperature vs. $I_{ratioed}$ plots. A trend line is used to sort areas into low Biot and high Biot areas based on the Biot number of a given location calculated as seen in Eqn. 14 reproduced below:

$$Bi = \frac{hL_c}{k} \tag{14}$$

The set of data comprising low Biot areas is used to determine the low Biot curve and the set of data comprising high Biot areas is used to determine the high Biot calibration. After applying the low Biot calibration for the low Biot areas and the high Biot calibration for the high Biot areas, data reduction for both sets occurs similarly, with the converted model surface temperature boundary condition entered into the existing 1-D Fourier heat equation code in use at Tunnel 9.

5.3: Technical Contributions

The contributions of this study are:

- Improved estimates and measures of TSP thermophysical properties, including estimates of TSP thermal conductivity based on tunnel data. These thermophysical properties were used in finite element models of TSP to analyze paint behavior, validate assumptions made in the data reduction process and perform a sensitivity analysis on system parameters. The sensitivity analysis indicated that amongst the studied parameters, paint thickness and thermal conductivity had the most effect on the heat transfer calculation. These models can allow for further analysis of paint behavior in more complex configurations or under more complex heat loads.
- The development of a Biot number vs. Reynolds number trend line to use as a sorting criterion, allowing for the objective selection of data used to determine calibration curves utilized in the data reduction process. The current trend line gave an equation for a sorting Biot number = 0.0014193 * Re#/ft (in millions) + 0.0001234. For a given location at a specific Re#/ft test condition, a Biot value greater than the sorting Biot number would be classified as a high Biot

value and a lower value would be classified as a low Biot value. Ongoing use of the TSP system will serve to grow and improve the database used to create the trend line.

- The development of a novel two calibration data reduction technique capable of reducing observed discrepancies in heat transfer results determined from TSP based measurements as compared to conventional thermocouple measurements, particularly for those areas of the test article with a high Biot number. For the runs where an improvement was seen in the high Biot locations in particular, the average discrepancy was reduced from 29% to 19% using the two calibration method.

5.4: Suggestions for Future Work

While there are promising results obtained from the use of the two calibration data reduction method to lower discrepancy between the thermocouple and TSP based heat transfer results, cases remain where the two calibration method does not address the observed discrepancies. The appeal of using the TSP system as a standalone heat transfer measurement tool is tempered if the measurements cannot reproduce results obtained from the existing thermocouple standard. The development of a TSP system that can reliably produce heat transfer results that are in good agreement with thermocouple based heat transfer results for all areas of the model instead of for most areas of the model is an important goal. As the Biot number sorting is used in more and more tunnel runs, the database on which to establish the trend line that determines the limiting Biot number used to identify high or low Biot areas should also grow. Ideally, this will lead to an improved trend line which will be

better able to sort model locations into the appropriate category and will improve the data reduction process. Ongoing research into the cause of exacerbated discrepancies caused by the two calibration method, as seen in Figure 27, also has the potential to produce further improvements in the data reduction process. In addition, continuing research into improved criteria for selecting the data used to determine the *in situ* calibrations can lead to additional accuracy in the TSP based heat transfer results as seen in Figure 28. For instance, objective determinations of where on the model and at what point during the run the flow is laminar or turbulent can greatly improve the estimate of the local convective heat transfer coefficient, *h*, and correspondingly, the Biot number estimate as well.

Furthermore, the data reduction process used here leverages existing code developed at Tunnel 9 for 1-D heat conduction normal to the model surface. However, it is desirable to transition to a more robust data reduction code that can operate in 2-D or 3-D environments as circumstances dictate. For example, sharp spatial heat-flux gradients, leading edges, fins, struts and other complex geometric features cannot be properly analyzed using 1-D conduction assumptions. Transitioning to a more robust code that can handle these phenomenon will extend the utility of the current TSP heat transfer measurement system.

Finally, a more accurate measure of the TSP thermophysical properties themselves may negate the need for an *in situ* thermocouple calibration process altogether. If the TSP thermophysical properties and thickness were well known at each location on the model, it would be feasible to determine heat transfer measurements without the need for thermocouple instrumentation at all. Also, it

would be possible to incorporate the TSP layer in the existing data reduction code without using an *in situ* calibration to determine what the model surface temperature underneath the paint layer would be. The TSP could be modeled in the code as a series of nodes with known properties, similar to the ANSYS simulations. Lab calibrations for TSP emission intensity could be used to determine TSP surface temperature. This TSP surface temperature would replace model surface temperature as one of the boundary conditions for the data reduction code and heat transfer results could be obtained in a similar manner as before. This would also negate the need for a linear temperature gradient assumption through the paint layer.

References

[1] MacLean, M. et. al. "Effect of Surface Catalysis on Measured Heat Transfer in an Expansion Tunnel Facility" 50th AIAA Aerospace Sciences Meeting. January 2012, Nashville, Tennessee.

[2] Capra, B. R. and Morgan, R. G., "Radiative and Total Heat Transfer Measurements to a Titan Explorer Model" Journal of Spacecraft and Rockets, Vol. 49, No. 1, January 2012

[3] Ward, C. A. C. et. al. "Hypersonic Boundary-Layer Transition Experiments in the Boeing / AFOSR Mach-6 Quiet Tunnel" 50th AIAA Aerospace Sciences Meeting. January 2012, Nashville, Tennessee.

[4] Kurits, I., "Quantitative Global Heat-Transfer Measurements Using Temperature-Sensitive Paint On A Blunt Body In Hypersonic Flows" Masters Thesis, University of Maryland, College Park.

[5] Watkins, A. N., et. al., "The Development and Implementation of a Cryogenic Pressure Sensitive Paint System in the National Transonic Facility" 47th AIAA Aerospace Sciences Meeting. January 2009. Orlando, Florida.

[6] Kurits, I., and Norris, J. "Hypersonic Global Heat-Transfer Measurements During Continuous Pitch Sweeps at AEDC Tunnel 9" 27th AIAA Aerodynamic Measurement Technology and Ground Testing Conference. June 2010. Chicago, Illinois.

[7] Hamner, M. P. et. al. "Using Temperature Sensitive Paint Technology" 40th Aerospace Sciences Meeting and Exhibit. January 2002, Reno, Nevada.

[8] Hamner, M. P., Norris, J. D. and Lafferty, J. F. "Recent Developments in TSP/PSP Technologies Focusing on High Velocity-Temperature and Non-Oxygen Environments" 24th AIAA Aerodynamic Measurement Technology and Ground Testing Conference. July 2004, Portland, Oregon.

[9] Roberts, G.T. and East, R.A. "Liquid Crystal Thermography for Heat Transfer Measurement in Hypersonic Flows: A Review" Journal of Spacecraft and Rockets, Vol. 33, No. 6, November – December 1996.

[10] Reda, D.C., Muratore Jr., J. J. and Heineck, J.T. "Time and Flow-Direction Responses of Shear-Stress-Sensitive Liquid Crystal Coatings" AIAA Journal, Vol. 32, No. 4, April 1994

[11] Blanchard, R. C., et. al. "Shuttle Orbiter Fuselage Global Temperature Measurements from Infrared Images at Hypersonic Speeds" AIAA Atmospheric Flight Mechanics Conference and Exhibit. August 2002. Monterey, California.

[12] Daryabeigi, K. "Global Surface Temperature/Heat Transfer Measurements Using Infrared Imaging" 17th AIAA Aerospace Ground Testing Conference. July 1992, Nashville, Tennessee

[13] Collier, A.S., Lafferty, J.F., Swinford, S.S., Witte, D.W. "Aerodynamic Heat Transfer Testing in Hypersonic Wind Tunnels using an Infrared Imaging System" 28th Aerospace Sciences Meeting, January 1990, Reno, Nevada.

[14] Micol, J.R. "Aerothermodynamic Measurement and Prediction for a Modified Orbiter at Mach 6 and 10 in Air" 26th Thermophysics Conference. June 1991, Honolulu, Hawaii.

[15] Allison, S. W., et. al. "Development of Temperature-Sensitive Paints for High-Temperature Aeropropulsion Applications" 37th AIAA/ASME/SAE/ASEE Joint Propulsion Conference and Exhibit. July 2001. Salt Lake City, Utah.

[16] Kafka, P. G., Gaz, J. and Yee, W. T. "Measurement of Aerodynamic Heating of Wind-Tunnel Models by Means of Temperature Sensitive Paint" Journal of Spacecraft and Rockets. Vol. 2. No. 3. 1965

[17] Hamner, M. P. "Demystifying Luminescent Paint Technology: A Guide for Non-Developers" 31st AIAA Fluid Dynamics Conference and Exhibit. June 2001. Anaheim, CA.

[18] Wadhams, T.P. et. al. "Experimental Studies of Space Shuttle Orbiter Boundary Layer Transition at Mach Numbers from 10 to 18" 48th AIAA Aerospace Sciences Meeting. January 2010. Orlando, Florida.

[19] Hubner, J. et. al. "Temperature and Pressure-Sensitive Paint Measurements in Short-Duration Hypersonic Flow" 37th AIAA Aerospace Sciences Meeting and Exhibit. January 1999. Reno, Nevada.

[20] Murphy, K. J. et. al. "Testing of the Crew Exploration Vehicle in NASA Langley's Unitary Plan Wind Tunnel" 45th AIAA Aerospace Sciences Meeting. January 2007. Reno, Nevada.

[21] Hamner, M.P., et. al. "Application of Temperature Sensitive Paint Technology to Boundary Layer Analysis" American Institute of Aeronautics and Astronautics Archive. 1997.

[22] Liu, T., Campbell, B. T. and Sullivan, J. P. "Thermal Paints for Shock/Boundary Layer Interaction in Inlet Flows" 28th Joint Propulsion Conference and Exhibit. July 1992. Nashville, Tennessee.

[23] Crafton, J., et. al. "Application of Temperature and Pressure Sensitive Paint to an Obliquely Impinging Jet" 37th AIAA Aerospace Sciences Meeting and Exhibit. January 1999. Reno, Nevada.

[24] Fey, U., Egami, Y. and Engler, R. H. "High Reynolds number transition detection by means of temperature sensitive paint" 44th AIAA Aerospace Sciences Meeting. January 2006. Reno, Nevada.

[25] Ragsdale, W.C. and Boyd, C.F., *Hypervelocity Wind Tunnel 9 Facility Handbook* Third Edition, NAVSWC TR 91-616, Silver Spring, MD, July 1993

[26] Norris, J. D., et. al. "Adapting Temperature-Sensitive Paint Technology for use in AEDC Hypervelocity Wind Tunnel 9" 24th AIAA Aerodynamic Measurement Technology and Ground Testing Conference. June 2004. Portland, Oregon.

[27] Liu, T. and Sullivan, J.P. *Pressure and Temperature Sensitive Paints,* Springer, New York, NY, 2005.

[28] Neely, A. J. and Tjong, W. C. "Calibration of Thermal Paints for Hypersonic Flight Test" 15th AIAA International Space Planes and Hypersonic Systems and Technologies Conference. April 2008. Dayton, Ohio.

[29] Liu, T., Campbell, B., and Sullivan, J.P. "Accuracy of Temperature-Sensitive Fluorescent Paint for Heat Transfer Measurements" 30th AIAA Thermophysics Conference. June 1995. San Diego, California.

[30] Cattafesta III, L. N., Liu, T. and Sullivan, J. P. "Uncertainty Estimates for Temperature-Sensitive Paint Measurements wuth Charge-Coupled Device Cameras" AIAA Journal Vol. 36, No. 11. November 1998.

[31] Kurits, I., Norris, J. D. and Bhandari, P. "Temperature-Sensitive Paint Calibration Methodology Developed at AEDC Tunnel 9" 49th AIAA Aerospace Sciences Meeting. January 2011. Orlando, Florida.

[32] Shimbo, Y. et. al. "Evaluation of Several Calibration Techniques for Pressure Sensitive Paint in Transonic Testing" American Institute of Aeronautics and Astronautics Archive. National Aerospace Laboratory, 1998. Japan.

[33] Strand, T. and Mateer, G.G. "A Comparison of Boundary-Layer Transition Data from Temperature-Sensitive Paint and Thermocouple Techniques" AIAA Journal. Vol. 8. 1970

[34] N. T. Smith, et. al. "Use of Temperature Sensitive Paint in AEDC Hypervelocity Wind Tunnel 9" 12th AIAA International Space Planes and Hypersonic Systems and Technologies Conference. December 2003. Norfolk, Virginia.

[35] Hubner, J.P. et. al. "Heat Transfer Measurements in Hypersonic Flow Using Luminescent Coating Techniques" 40th AIAA Aerospace Sciences Meeting. January 2002, Reno, Nevada.

[36] Liu, T., et. al. "Analytical Method for Determining Heat Flux from Temperature-Sensitive Paint Measurements in Hypersonic Tunnels" Journal of Thermophysics and Heat Transfer. Vol. 24, No. 1. January 2010.

[37] Liu, T., Campbell, B. and Sullivan, J.P. "Remote Surface Temperature and Heat Transfer Mapping for a Waverider Model at Mach 10 Using Fluorescent Paint" 18th AIAA Aerospace Ground Testing Conference, June 1994, Colorado Springs, Colorado.

[38] Liu, T. et. al. "Analytical Methods for Determination of Heat Transfer Fields from Temperature Sensitive Paint Measurements in Hypersonic Tunnels" 47th AIAA Aerospace Sciences Meeting. January 2009, Orlando, Florida.

[39] Campbell, B.T. et. al. "Temperature Sensitive Fluorescent Paint Systems" 18th AIAA Aerospace Ground Testing Conference, June 1994, Colorado Springs, Colorado.

[40] Schairer, E. T. et. al. "The Effects of Thin Paint Coatings on the Aerodynamics of Semi-Span Wings" American Institute of Aeronautics and Astronautics Archive. NASA Ames Research Center, 1998. Moffet Field, California.

[41] Kurits, I and Lewis, M. J. "Global Temperature-Sensitive Paint System for Heat Transfer Measurements in Long-Duration Hypersonic Flows" Journal of Thermophysics and Heat Transfer. Vol. 23, No. 2 April 2009.

[42] Boyd, C. F. and Howell, A. "Numerical Investigation of One-Dimensional Heat-Flux Calculations" Dahlgren Division, Naval Surface Warfare Center, October 1994, Silver Spring, Maryland.

[43] Nagai, H., Ohmi, S. and Asai, K. "Effect of Temperature Sensitive Paint Thickness on Global Heat Transfer Measurement in Hypersonic Flow" Journal of Thermophysics and Heat Transfer. Vol. 22, No. 3 July 2008

[44] Eckert, E.R.G. "Engineering Relations for Heat Transfer and Friction in High-Velocity Laminar and Turbulent Boundary-Layer Flow over Surfaces With Constant Pressure and Temperature" Transaction of the American Society of Mechanical Engineers. Vol. 78, No. 6 August 1956. pg. 1273.

[45] Anderson, Jr., J.D. *Hypersonic and High-Temperature Gas Dynamics.* Second Edition, AIAA, Reston, VA. 2006